

THE PRESSURE - INDUCED FUNDAMENTAL BAND
OF OXYGEN IN PURE GAS AND IN OXYGEN
FOREIGN GAS MIXTURES AT 298°K AND AT 201°K

CENTRE FOR NEWFOUNDLAND STUDIES

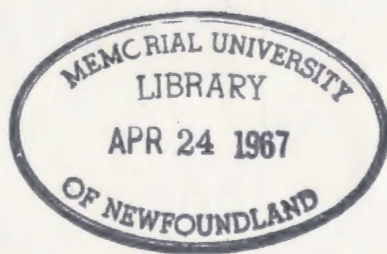
**TOTAL OF 10 PAGES ONLY
MAY BE XEROXED**

(Without Author's Permission)

ROBERT B. BISHOP

THE UNIVERSITY OF CHICAGO
LIBRARY

1952





THE PRESSURE - INDUCED FUNDAMENTAL BAND
OF OXYGEN IN PURE GAS AND IN OXYGEN - FOREIGN
GAS MIXTURES AT 298⁰K and at 201⁰K

by

Robert B. Bishop, B.Sc (Hons.)

Submitted in partial fulfilment
of the requirements for the degree of Master of Science
Memorial University of Newfoundland

September 1966

i

ERRATA

Page 68, line 8:- "McDonald, R. E." should read:

"MacDonald, J. C. F."

This thesis has been examined and approved by:

External Examiner: Dr. J. L. Hunt,
Assoc. Prof. of Physics,
University of Guelph,
Guelph, Ontario.

Internal Examiner: Dr. S. P. Reddy,
Asst. Prof. of Physics,
Memorial University of Newfoundland.

TABLE OF CONTENTS

CHAPTER	Page
	ABSTRACT 1
I	INTRODUCTION 2
II	EXPERIMENTAL 6
	Gas Absorption Cell 6
	Optical Arrangement 11
	Purifying System 14
	Experimental Procedure 18
III	EXPERIMENTAL RESULTS 22
	(1) The Room Temperature Experiments ... 22
	The Absorption Profiles 22
	The Absorption Coefficients 24
	(2) The Low Temperature Experiments..... 36
	The Absorption Profiles..... 36
	The Absorption Coefficients 44
IV	THEORY AND DISCUSSION 50
	Outline of Theory 50
	Calculation and Discussion of Results.. 57
	REFERENCES 66
	ACKNOWLEDGEMENTS..... 69

ABSTRACT

The pressure - induced fundamental vibration - rotation absorption band of oxygen was studied in the pure gas and in an oxygen - argon mixture at 298°K and in the pure gas and in oxygen nitrogen, oxygen-argon mixtures at 201°K at total pressures up to 300 atmospheres. The absorption profiles obtained in each case showed the pronounced Q and S branches with an indication of the less resolved O branch. The integrated absorption coefficients obtained from the absorption profiles were found to follow an empirical power series in terms of the partial densities of the component gases. A plot of $(1/p_a) \int \alpha(\nu) d\nu$ vs. p_a for pure oxygen and of $(1/p_a p_b) \int \alpha_{ab}(\nu) d\nu$ vs. p_b for mixtures was found to be a straight line from which the binary and ternary absorption coefficients were determined. Applying the theory of Van Kranendonk it was found that the overlap contribution to the binary absorption coefficient was negligible and from the known molecular constants the derivative of the molecular quadrupole moment of oxygen, Q' , with respect to the internuclear distance at the equilibrium position was determined. The value of Q' obtained was $1.6 ea_0$ which is equal to that determined by Shapiro and Gush (1966).

CHAPTER I

INTRODUCTION

The investigation of the absorption bands of oxygen under pressure was first carried out by Janssen (1886) who found that the visible absorption bands of compressed oxygen gas vary quadratically with the pressure. A number of investigations on the many absorption bands of oxygen in various optical regions have been made since then and have revealed some of the properties of the oxygen molecule. The existence of $(O_2)_2$ complexes in liquid oxygen was postulated by Lewis (1924) on the basis of magnetic susceptibility measurements of liquid oxygen-nitrogen mixtures. Assuming the presence of these $(O_2)_2$ complexes in gaseous oxygen, the quadratic pressure dependence of the absorption intensity could be explained. Oxygen molecules are different from other diatomic molecules in that a pair of unpaired orbital electrons gives a net spin of unity, resulting in the triplet electronic ground state, $^3\Sigma_g^-$, and the paramagnetism of the molecule which led to the postulate of the existence of $(O_2)_2$ molecular complexes.

Since the oxygen molecule has no permanent electric dipole moment, no infrared absorption spectrum can be expected. However, in an attempt to detect $(O_2)_2$ complexes by infrared absorption, Crawford, Welsh and Locke (1949) found an absorption at the fundamental vibrational frequency of the O_2 molecule in liquid and compressed gaseous oxygen. Their investigation showed

that the absorption can be induced by the intermolecular forces acting during the collisions of the molecules.

The fundamental absorption band of oxygen was also investigated by Smith, Keller and Johnston (1950, 1952) in liquid and solid oxygen. They found an anomaly in the absorption spectrum which they interpreted as originating in the infrared-active out-of-phase coupled oscillation of two associated O_2 molecules, $(O_2)_2$.

The first overtone of the pressure induced fundamental absorption band of oxygen was studied by Welsh et al (1951) and the second overtone band by Gush (1956). There are several band systems of oxygen observed in the visible optical region known as the "combination" bands which are noted for their importance to the postulate of the $(O_2)_2$ complexes. Fourteen of these absorption bands of compressed gaseous oxygen, in the region 6300 \AA to 3150 \AA , have been studied by many investigators. Ellis and Kneser (1933) showed that the frequencies of the band maxima could be represented by the formula,

$$\nu_{\max} = m\nu_1 + n\nu_2 + \nu\omega$$

where (m,n) has the values $(2,0)$, $(1,1)$ and $(0,2)$ and $\nu = 0,1,2, \dots$, ν_1 and ν_2 are the frequencies of the $(0,0)$ bands of the electronic transitions ${}^1\Delta_g - {}^3\Sigma_g^-$ and ${}^1\Sigma_g^+ - {}^3\Sigma_g^-$ respectively and ω has a value of the order of 1450 cm^{-1} . Hence, the band systems have been assumed to arise from the simultaneous electronic transitions of two oxygen molecules. Ellis and Kneser assumed that this absorption was due to loosely bound $(O_2)_2$ complexes; the assumption

was also valid for the explanation of the quadratic dependance of the absorption intensity on pressure. However, this quadratic dependance can be explained in terms of the collision induced absorption.

The first direct evidence of the presence of molecular complexes at low temperatures was recently obtained by Watanabe and Welsh (1964) in hydrogen gas. In their experiments at temperatures lower than 40°K the infrared absorption spectrum of hydrogen was accompanied by a number of resolved sharp lines, an analysis of which showed that the lines could unquestionably be interpreted as transitions involving bound and virtual states of $(H_2)_2$ complexes. Their calculations showed that the two bound states of the $(H_2)_2$ complex could have sufficient population at low temperatures to cause a sharp rise in the absorption coefficient as the temperature decreased below 30°K.

The theory of the pressure induced fundamental band of homonuclear diatomic molecules proposed by Van Kranendonk (1957, 1958) has been applied successfully in the interpretation of experimental results obtained by a number of investigators of pressure induced absorption bands. This theory is based on the assumption that the absorption induced by binary collisions arises from (1) an electron overlap interaction in which the electric dipole moment induced in an absorbing molecule decreases exponentially with the intermolecular distance r , and (2) a

molecular quadrupole interaction in which the induced electric dipole varies as R^{-4} . According to this so called "exp-4" model the electric dipole moment induced by the short range overlap forces is to a first order approximation independent of the relative orientations of the molecules in a colliding pair and produces mainly transitions for which $\Delta J=0$, giving rise to the Q branch of the absorption band. The long range quadrupole interaction, however, is strongly dependant on relative orientations of the colliding molecules and produces transitions for which $\Delta J = \pm 2$, giving rise to the S and O branches, as well as $\Delta J=0$ or the Q branch.

In the present investigation, the pressure induced fundamental absorption band of oxygen was studied in pure oxygen, oxygen-argon mixtures at room temperature (298°K), and in pure oxygen, oxygen-nitrogen and oxygen-argon mixtures at dry-ice temperature (201°K), with total pressures up to 300 atmospheres. From the experimental results, the binary and ternary absorption coefficients were determined and presented in Chapter III. The theory proposed by Van Kranendonk was applied for the analysis of the results obtained, and a general discussion is given in Chapter IV.

Chapter II

Experimental

Gas Absorption Cell

A 1 m transmission type absorption cell was used in the present investigation at pressures up to 300 atm. and at temperatures of 298°K and 201°K. A diagram showing the construction of one end of the cell is given in Fig. 1. The cell body, A, of stainless steel tubing has an inner bore of 3/4 inches diameter with a wall thickness of 1/8 inches and 1 metre in length with two flanges, L, hard-soldered at both ends. The end pieces, B, also of stainless steel are 3 inches in diameter and are attached to the cell body by means of the steel closing nuts, N. A pressure tight fit is obtained at the stainless steel ring, R, between the end piece, B, and the flange, L, of the cell body.

Inserted into the bore of the cell body were four sections of a hollow stainless steel cylinder, G, each section consisting of two parts and having a central bore of rectangular cross-section 0.2 inches by 0.4 inches. These four sections were keyed together to insure proper alignment of the central bore and served as a light guide for the cell. The inside surfaces of the bore were polished to give good reflection of light.

The exit and entrance windows, W, were polished sodium chloride plates 1 inch in diameter and 3/4 inch thick. They were cemented to the stainless steel window plates, P, with a silicone sealant. To ensure a good pressure seal, the surface

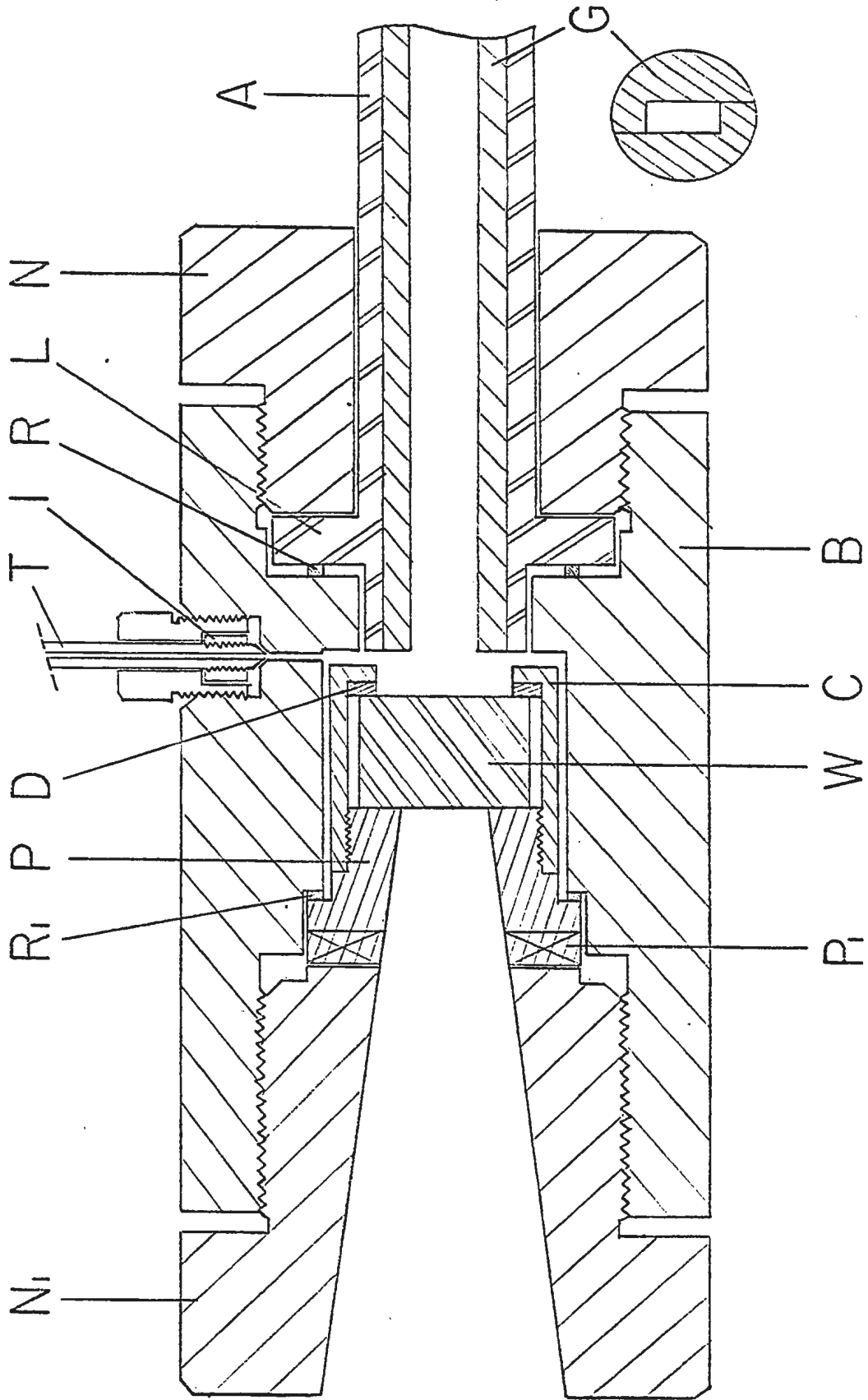


Fig. 1 End-piece of gas absorption cell.

of the window plates on which the window was cemented was polished optically flat. The windows were secured by steel caps, C, with teflon washers, D, so that the cell could be evacuated without the windows becoming loose. The aperture of the window plates was rectangular having dimensions 0.2 inches by 0.5 inches.

A pressure tight fitting was made between the window plate, P, and the end piece, B, by means of the closing nut, N_1 and a stainless steel ring, R_1 . The portion, P_1 of the window plates, 0.2 inches thick, was square in shape and fitted into a matched recess of the end piece in order to prevent a misalignment of the light guide and window plate aperture when the closing nut, N_1 , was tightened.

A 1/4 inch diameter stainless steel capillary tube, T, served as a gas inlet to the cell and was connected by an "Aminco" fitting, I.

For the low temperature experiments a cylindrical galvanized sheet steel "jacket", 3 3/8 inches in diameter was placed around the cell, as shown in Fig. 2, to contain the coolant consisting of dry-ice and ethyl alcohol. This "jacket" was sealed around the end pieces of the cell body by means of neoprene "O" rings. The coolant was placed around the cell through two funnels attached to the "jacket". The system was insulated by a two inch thick layer of styrofoam surrounding the cooling "jacket". In order to prevent frosting on windows during the low-temperature experiments, a vacuum chamber, constructed of Plexiglass, was attached to each of the end pieces of the cell. In Fig. 3 the attachment of the vacuum chamber to the cell is shown. A neoprene "O" ring, A, was used to secure a vacuum seal between

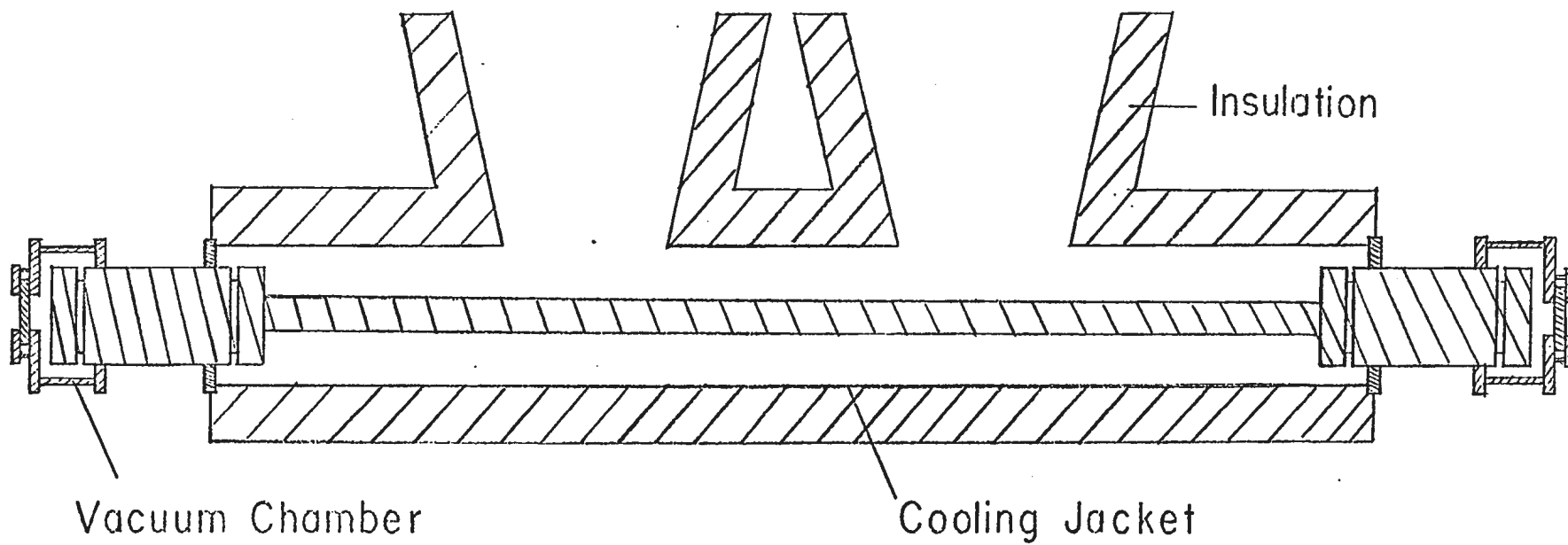


Fig. 2 Insulated cooling jacket and absorption cell.

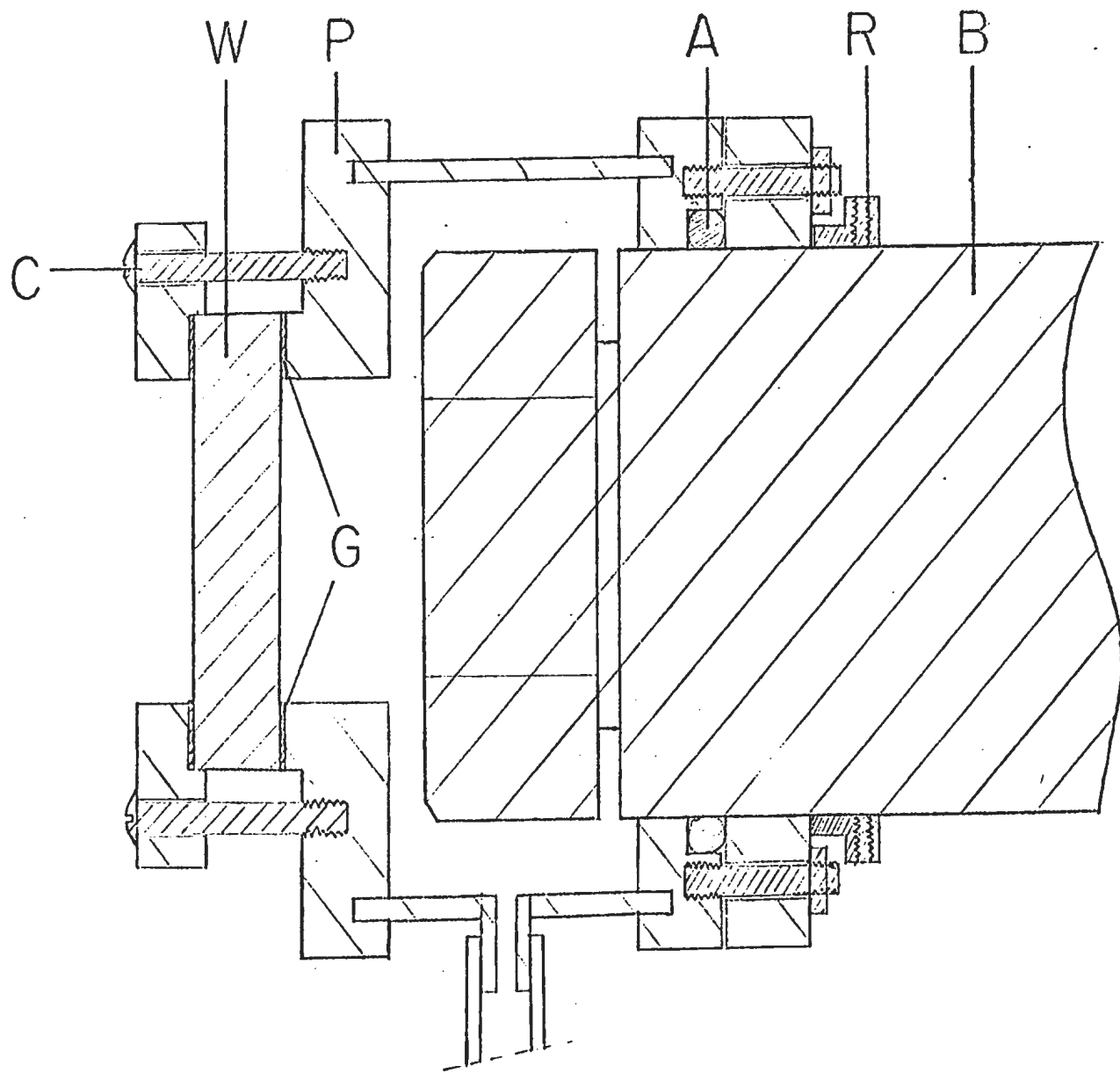


Fig. 3 Vacuum chamber attachment to the absorption cell.

each chamber and end piece of the absorption cell. Retaining rings, R, were fastened by means of set screws to keep each vacuum chamber from slipping on over the end piece of the cell when the chamber was evacuated. A sodium chloride plate, W, 1 inch by 2 3/8 inches by 1/2 inch sealed to the Flexiglass frame, P, by means of the clamping arrangement, C, and a rubber gasket, G, served as a secondary window; the secondary entrance and exit windows were maintained at room temperature by evacuating the chambers.

The optical path length of the cell used was 102.4 cm for the room temperature experiments and 102.2 cm for the low temperature (201°K) experiments. The correction to the path length due to the reflection inside the light guide was found to be negligible.

Optical Arrangement

The optical system used with the transmission cell is shown schematically in Fig. 4. Infrared radiation from the source, S, was focussed on the entrance window of the cell, H, by means of an aluminized spherical front surface mirror, M. The radiation from the exit window was then focussed on to the slit, S, of the spectrometer, A, by means of a second spherical mirror, M₂, and a plane mirror, M₃. An F/4 light cone was used throughout the external arrangement to match the internal optics of the spectrometer.

A Perkin-Elmer model 99-G double pass grating spectrometer with a grating of 6μ blaze wavelength, along with a Golay pneumatic infrared detector were used to study the absorption spectra in the present investigation. A water cooled globar operated

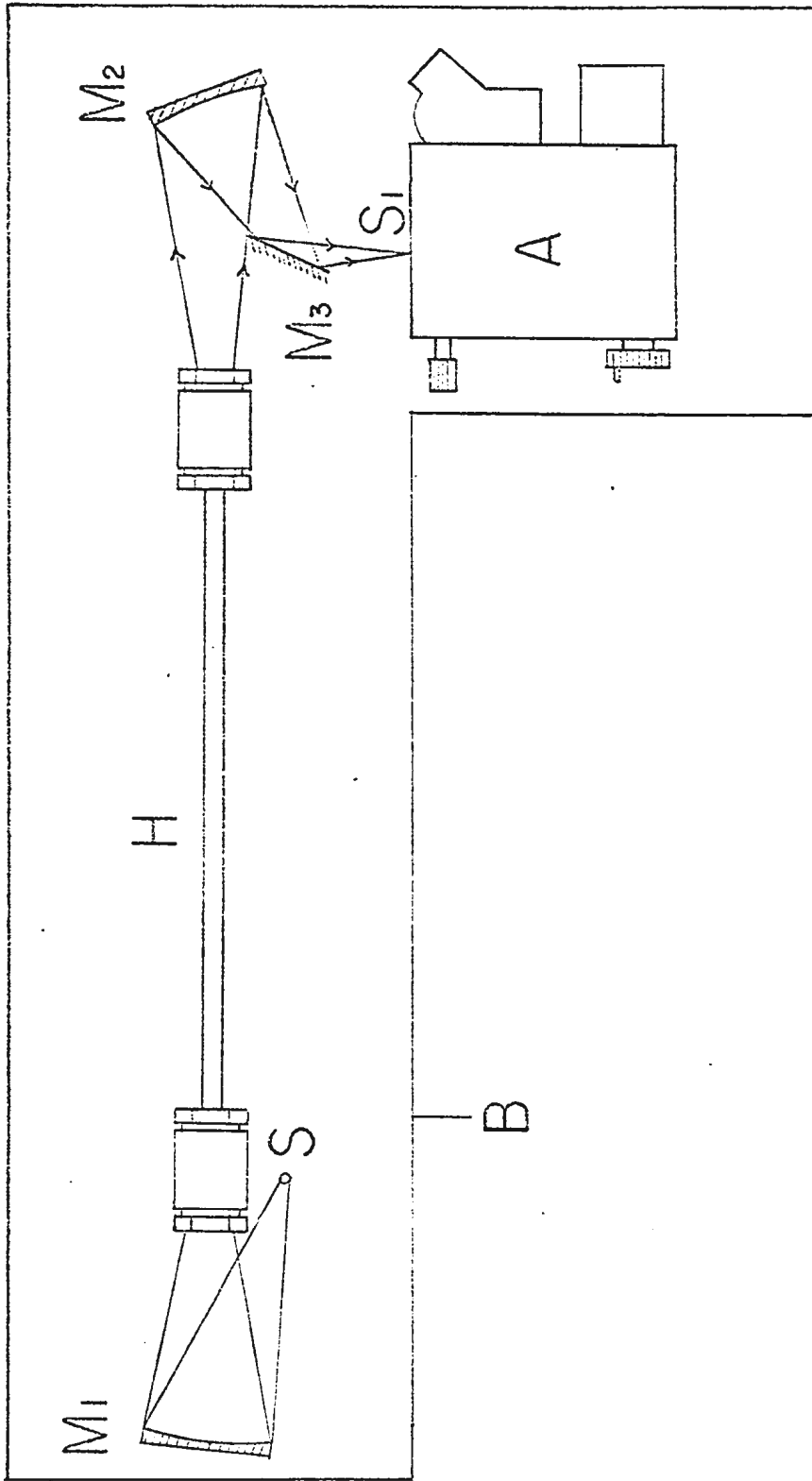


Fig. 4 Optical arrangement

at a power of approximately 125 watts from a Sorensen voltage regulator was used as the source of infrared continuum. The slit width of the spectrometer was set at 2.0mm. which gave a spectral slit width of 5.3 cm^{-1} at 1556 cm^{-1} , the origin of the fundamental band of oxygen.

Since the pressure induced fundamental absorption band of oxygen lies in the region of a strong absorption band of water, it was necessary to keep the entire optical path outside the absorption cell free from water vapor. To do this, a fairly extensive flushing system was used. A large polyethylene bag was constructed by heat sealing sections together around an aluminum framework. This framework which was approximately one foot high surrounded the optical arrangement of absorption cell, spectrometer and source as outlined by, A, of Fig. 4. With the optical arrangement thus enclosed in this air-tight bag, the humidity inside could be kept at a minimum level by flushing the bag with dry air. All connections to the system such as wiring to the spectrometer and high pressure tubing to the cell were passed through the enclosure through purposely constructed polyethylene sleeves which were then tied over to form an air tight seal. To operate the grating drive and slit control mechanism of the spectrometer, a polyethylene "glove" was sealed to the bag so that these operations could be made without exposing the optical path to the room atmosphere.

The dry air for the flushing system was obtained by passing compressed atmospheric air through a series of drying traps. It was first passed through silica gel and Drierite (CaSO_4)

traps to remove the bulk of the moisture in the air, then passed through a low temperature trap cooled by liquid nitrogen where most of the remaining moisture was condensed and finally passed through a phosphorous pentoxide trap. This dried air was then introduced to the polyethylene bag in two places, one near the globar source, Fig. 4, and one directly into the spectrometer. The escaping air from inside the bag was allowed to exit at a remote corner. A manometer was used to control the flow rate into the bag so that it could be kept constant at all times during an experiment. A flow rate of approximately 1 ft.³/min. was used for each experiment. This arrangement reduced the intensity of water absorption in the background absorption spectrum almost to the noise level.

Purifying System

As previously mentioned, a strong water absorption band lies in the same region (6μ) as does the fundamental absorption band of oxygen. This made it necessary to remove water vapor from the oxygen and perturbing gases as thoroughly as possible before introducing them to the cell, otherwise the measured absorption spectrum would be due to a combination of oxygen and water absorption bands.

A schematic diagram of the purifying system is shown in Fig. 5. The system is a network of high pressure valves, gauges and thermal compressors which are connected by 1/4 inch stainless steel capillary tubing except the portion between the valves

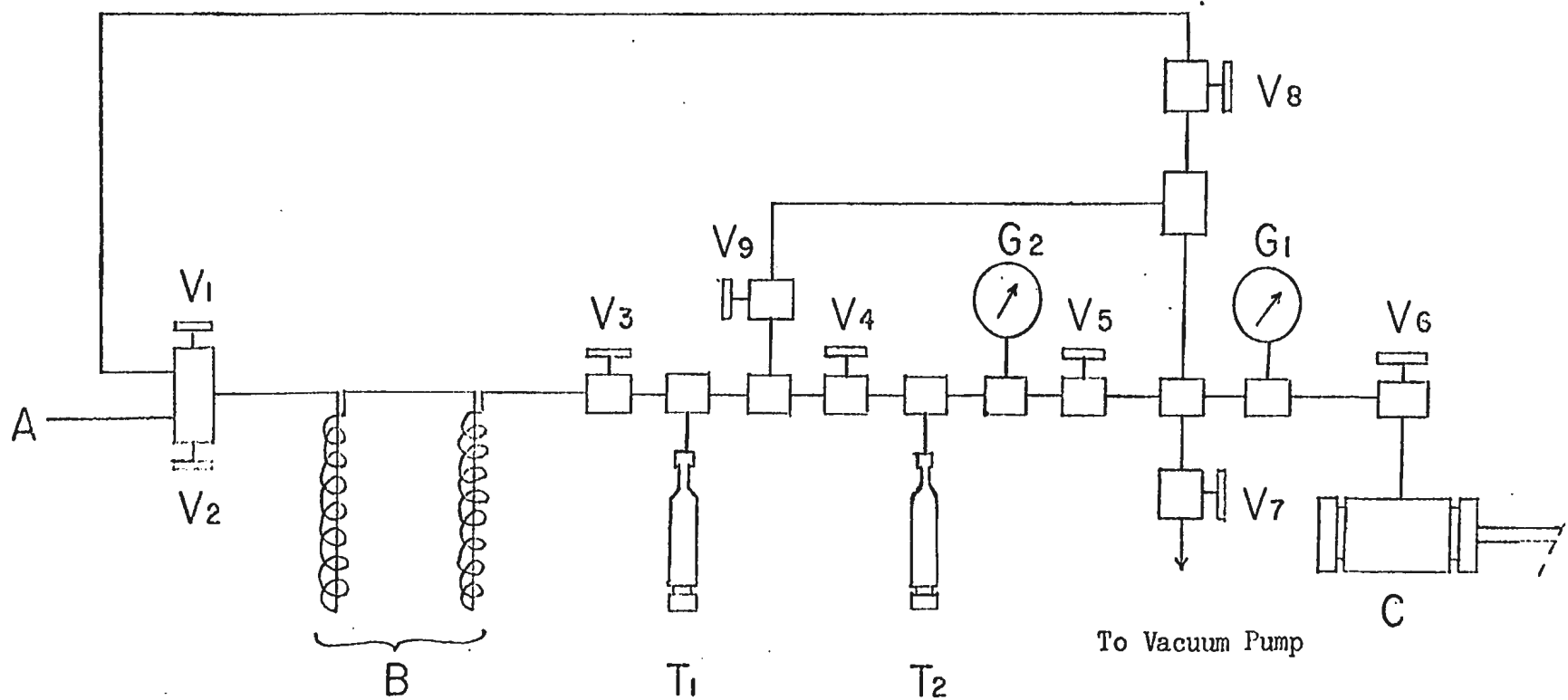


Fig. 5 High pressure gas system.

V_1 and V_3 . This system was used to prepare the oxygen and perturbing gases before they were introduced to the absorption cell at different pressures.

The procedure used to purify the oxygen was as follows: Oxygen gas from a commercial cylinder was introduced at a point, A, of the previously evacuated high pressure system, Fig. 5. While valves V_1 , V_5 , V_6 , V_7 , V_8 , and V_9 were closed, the oxygen was allowed to pass very slowly through the two low temperature traps, B. These traps consisted of coils of 1/4 inch copper tubing and were surrounded by frozen or viscous ethyl alcohol giving a temperature of approximately -115°C . The oxygen was condensed in the liquid nitrogen cooled thermal compressor, T_2 . The valve, V_4 , was then closed and the traps B which were brought to room temperature were evacuated through valve V_7 by opening valves V_1 and V_8 . The oxygen gas was then allowed to pass slowly from the compressor T_2 to the compressor T_1 through the valves V_5 , V_8 , V_1 and V_3 so that it passed through the cold traps, B, for the second time. By means of controlling the valves, the oxygen gas was transferred back and forth between T_1 and T_2 , each time the gas being passed through the cold traps.

It was found that after the oxygen was passed three times through the traps, B, no detectable absorption of the water bands could be observed when about 1200psi. of oxygen was introduced to the cell. However, to make certain that no water band would interfere with the oxygen absorption, the oxygen gas was passed through the traps, B, six times prior to

its use in the absorption cell. The purified oxygen was then stored in the thermal compressor T2 with the valves V4, V5, and V8 closed. The pressure inside the compressor was measured by means of the 0-5000 psi. Bourdon tube-type pressure gauge, G2.

The perturbing gases nitrogen and argon, which were found to contain much less water vapor than oxygen gas, were dried by passing them very slowly through the previously described low temperature traps, B, and collected in the thermal compressor T1. These gases were then introduced to the cell through valves V9 and V6. Each of the perturbing gases nitrogen and argon was admitted to the absorption cell alone and its spectrum was observed prior to each experiment to ensure the absence of water vapor contamination.

Helium gas was also used in a mixture experiment with oxygen, however, no measureable absorption intensity was observed for total pressures up to 3000 psi., a result which will be discussed in Chapter IV.

EXPERIMENTAL PROCEDURE

Prior to each experiment the following procedures were carried out: The electronics of the spectrometer system were turned on at least twelve hours before any measurements were taken so that the system reached maximum stability; the optical system was flushed continuously with dry air for several hours before measurements were taken and continued for the duration of the experiment; the absorption cell was evacuated for several hours; for the low temperature experiments, the vacuum chambers protecting the cell windows were evacuated and the cell cooled down to 201°K by surrounding the cell with a mixture of ethyl alcohol and dry-ice. After the above procedures were followed, several recorder traces were taken until a good reproduction of the background spectrum was obtained.

For the pure oxygen experiments, the oxygen was introduced to the cell through valves V5 and V6 of Fig. 5. The pressure inside the cell was measured by the 0-5000 psi. Bourdon tube-type gauge G, which was calibrated against an Ashcroft dead weight pressure balance. For each pressure used, recorder traces were taken until good reproduction of the absorption spectrum was obtained.

For the gas mixture experiments the so called "constant base density" method was employed. Oxygen gas at the required pressure was first introduced to the evacuated absorption cell from the thermal compressor T2 and the absorption spectrum was obtained. The valves V5 and V6 were then closed and the capillary tubing bounded by valves V5, V6, V7, V8, and V9 was

evacuated through valve V7. In admitting the perturbing gas to the cell, the valve V9 was first opened and the pressure was allowed to rise as determined by the gauge G_1 by slowly heating the compressor T1. When sufficient pressure difference was reached between the pressure inside and outside the cell, the valve V6 was used to admit the perturbing gas by means of a series of short pulses preventing the back diffusion of the gas from the cell. About 20 to 30 minutes were allowed for proper mixing to take place, then recorder traces were taken until good reproduction was obtained. The length of the stainless steel capillary tubing between valve V6 and the cell was made as short as possible to minimize the error caused by inhomogeneous mixing inside it.

Following the above procedures, oxygen-perturbing gas mixture experiments were carried out using a constant base density of oxygen at a series of total pressures. The highest total pressure used in the present study was approximately 300 atmospheres, and the initial base pressure of oxygen was in a range of approximately 12 to 33 atmospheres.

To calculate the densities of the various gases, isothermal data was obtained from the following sources; Michels, Schamp, and de Graaff (1954) for oxygen at 298°K up to 130 atmospheres, Amagot (1893) for higher pressures of oxygen at 298°K ; Michels, Wijker, and Wijker (1949) for argon at 298°K ; Hilsenrath et al (1955) for oxygen, argon and nitrogen at 201°K . While the densities of pure oxygen at various pressures may be directly computed from the above isothermal

data, the partial densities of the perturbing gases cannot be estimated directly. The following interpolation method was therefore used to determine the partial density of the perturbing gas. An approximate value for the partial pressure of the perturbing gas was obtained by subtracting the "base" pressure of oxygen from the total pressure of the mixture, the assumption being that the partial pressures of the component gases were additive. The approximate partial density was then determined from the previously mentioned isothermal data, and the approximate mixture ratio $\beta' = \rho_b' / \rho_a$ was calculated, where ρ_b' is the approximate partial density of the perturbing gas and ρ_a is the partial density of oxygen. Then, using the equation (1)
$$\rho_b = \frac{1}{1+\beta'} \{ (\rho_a)_p + \beta' (\rho_b)_p \} - \rho_a$$
 the partial density ρ_b of the perturbing gas was calculated. Here $(\rho_a)_p$ and $(\rho_b)_p$ are the densities of oxygen and perturbing gas respectively at the mixture pressure P.

A similar method for calculating the partial density of a perturbing gas in a mixture was used by Cho et al (1963) and Pai (1965) and its accuracy found to be within the limit of experimental error. The densities were expressed in Amagot units which are defined as the ratio of the density at a given pressure and temperature to the density at N.T.P.

For the measurement of the absorption contours, the grating spectrometer was calibrated for the region 1300 cm^{-1} to 1000 cm^{-1} using the known frequencies of the water bands appearing in this region (Thomson, 1961). From the absorption spectrum as obtained on the recorder trace, an absorption contour was

obtained by plotting the absorption coefficient, $\alpha(\nu)$ as a function of the frequency ν in cm^{-1} . The absorption coefficient, $\alpha(\nu)$, is given by $1/L \log_e (I_0/I)$, where I is the intensity of radiation after it has passed through an absorbing path of length, L , and I_0 is the background intensity of radiation at the same frequency but with no absorbing medium in the path. The integrated absorption coefficient of the absorption band, $\int \alpha(\nu) d\nu$ in cm^{-1}/cm was determined by computing the area under the absorption contour.

In the gas mixture experiments, the "enhancement" absorption contour was obtained by plotting $\alpha_{en}(\nu)$ as a function of the frequency ν in cm^{-1} . The enhancement absorption coefficient $\alpha_{en}(\nu)$ is given by $1/L \log_e (I_1/I_2)$ where I_1 , is the intensity transmitted by the cell filled with the pure oxygen at the base density only and I_2 is the intensity with the mixture in the cell. The enhancement in the integrated absorption coefficient, $\int \alpha_{en}(\nu) d\nu$

is obtained by subtracting the area under the absorption contour of the pure oxygen alone from that of the gas mixture.

Chapter III

Experimental Results

(1) The Room Temperature Experiments

The Absorption Profiles

Observed absorption profiles of the fundamental band of oxygen in pure gas at $T=298^{\circ}\text{K}$ are presented in Fig. 6. They show pronounced Q and S branches, corresponding to the transitions $\Delta J = 0, +2$ and an indication of the O branch for which $\Delta J = -2$. Here J is the rotational quantum number. The positions of the band origin, ν_0 , at 1556 cm^{-1} and the maxima in the O and S branches as calculated from the known molecular constants of free oxygen molecules (Herzberg, 1950) have been marked on the frequency axis and agree well with the observed positions. In order to compare the profiles at different densities, absorption contours of several densities were normalized in such a way that the areas under the contours were made equal. It was found that these normalized contours showed no appreciable change in the overall shape or in the positions of the branch maxima for the present range of densities.

The positions of the individual rotational lines of the quadrupole spectrum of the band are also shown in Fig. 6 for the purpose of comparison. Since the nuclear spin $I=0$ and the ground electronic state is $^3\Sigma_g^-$ for oxygen, only the rotational transitions between odd or symmetric rotational levels will appear since all the even or antisymmetric rotational levels will be missing. The length of each rotational line as shown is

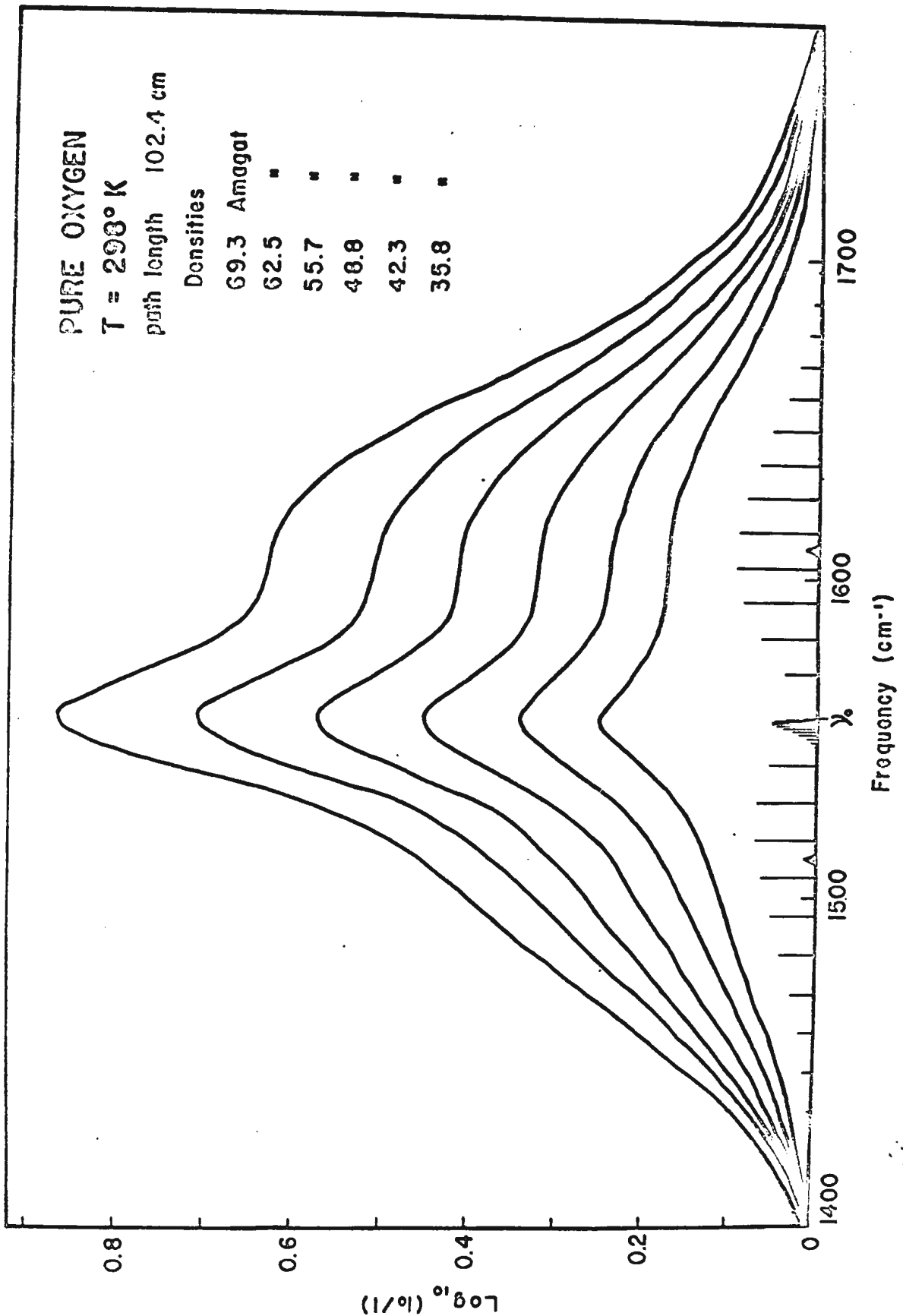


Fig. 6 The fundamental absorption band of oxygen at 298°K at various densities of gaseous oxygen. The triangular marks on the frequency axis, on the left and right sides of ν_0 , represent O_{\max} and S_{\max} respectively.

drawn proportional to the absorption intensity of the corresponding rotational quadrupolar transition in the fundamental band.

As seen in Fig. 6 the general feature of calculated quadrupolar absorption agrees well with the observed shape.

A set of observed enhancement absorption profiles in an oxygen-argon mixture is presented in Fig. 7. These contours show no appreciable shift in the positions of the O, Q, and S branch maxima. From a normalization of a selection of contours it was found that the shape of absorption band remained the same at different densities.

A comparison of the absorption profile of pure oxygen and the enhancement absorption profile of the oxygen-argon mixture is shown in Fig. 8. The profiles were so chosen that the product of the partial densities, $\rho_{O_2} \rho_A$ and $\rho_{O_2}^2$, were approximately the same for each contour. This procedure was followed in order to compare the overall absorption arising from the binary collisions of the molecules. The oxygen - argon mixture contour shows a considerable sharpening in the region of the Q branch relative to the O and S branches as compared with the Q branch for the pure oxygen contour, and also, the magnitude of the total absorption is greater for pure oxygen than for the oxygen-argon mixture.

The Absorption Coefficients

The observed integrated absorption coefficients for pure oxygen and oxygen-argon mixtures are summarized in Tables I and II.

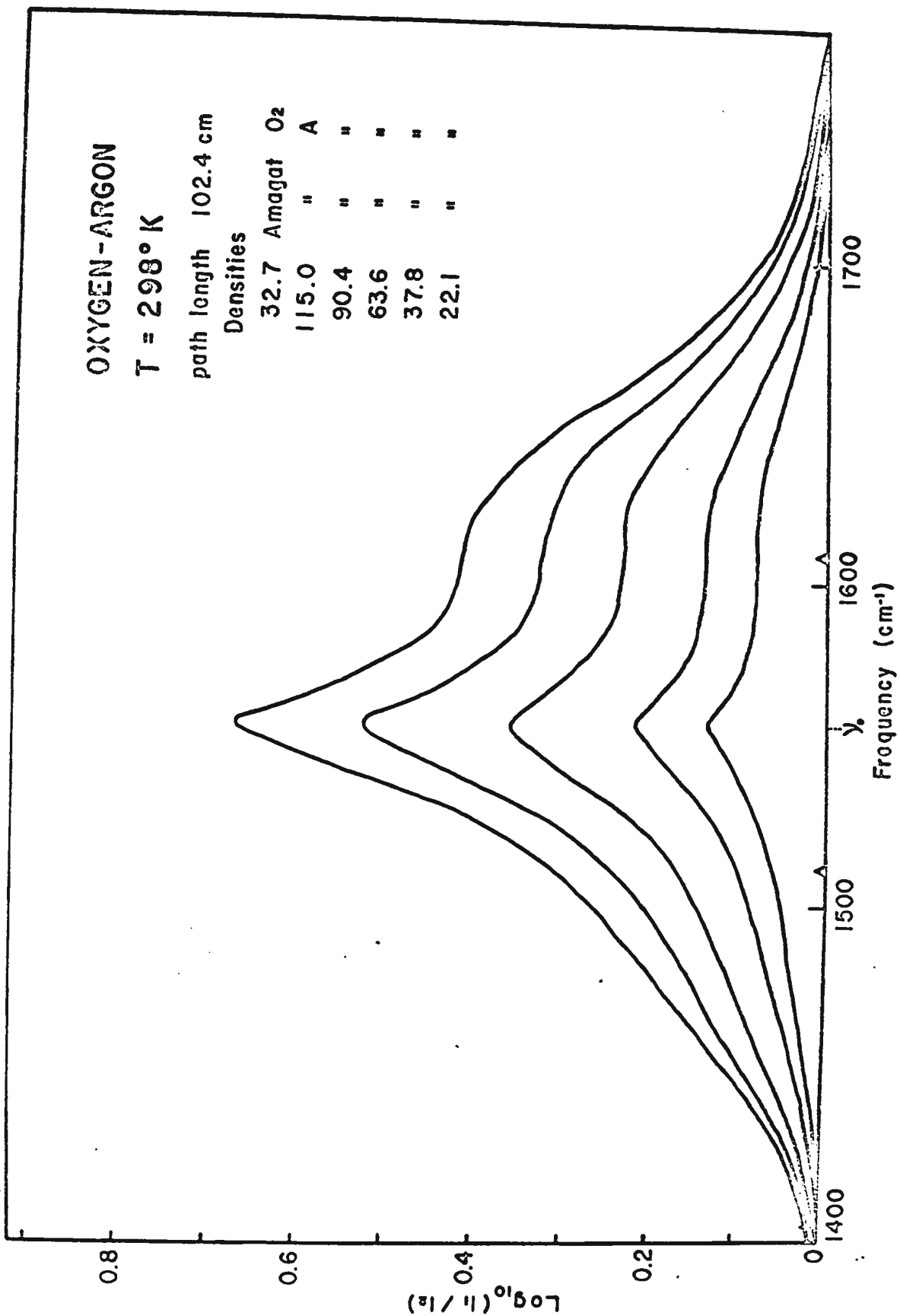


Fig. 7 Enhancement of the absorption of the fundamental band of oxygen at 298° K in an oxygen - argon mixture.

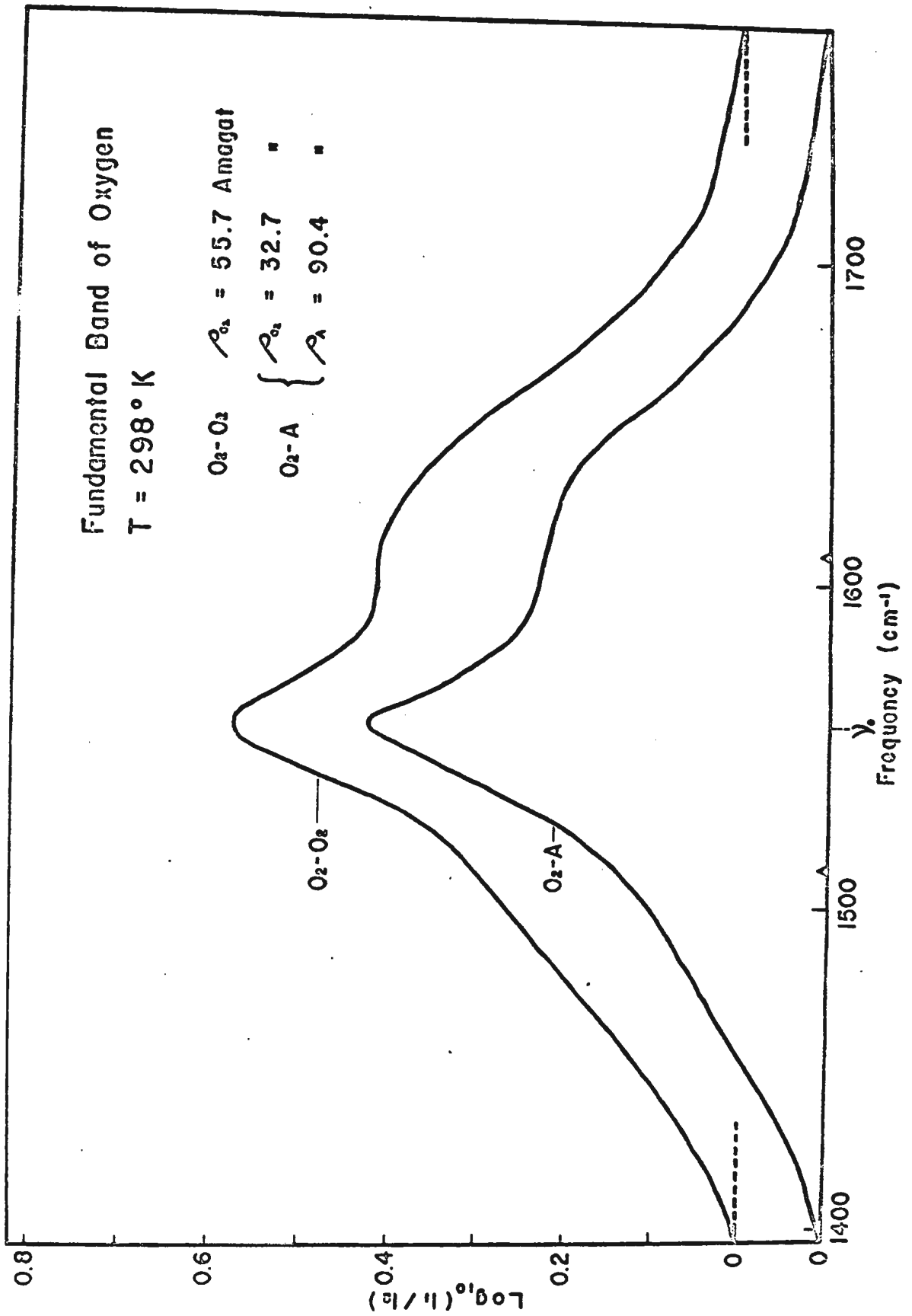


Fig. 8 The fundamental absorption band of oxygen at 298°K in pure oxygen and in an oxygen - argon mixture.

Table I
Summary of Results
Pure O₂ , T = 298°K

P_{O_2} (Amagat)	$\int \alpha(\nu) d\nu$ (cm ⁻¹ /cm)
25.9	0.481
29.1	0.508
32.7	0.755
32.7	0.678
35.8	0.817
39.3	1.059
42.3	1.143
45.8	1.414
48.8	1.521
52.6	1.817
55.7	1.944
59.6	2.314
62.5	2.391
65.8	2.674
69.3	2.950
72.6	3.257
79.6	4.020

Table II
Summary of Results
O₂ - A Mixture , T = 298°K

P_{O_2} (Amagat)	P_A (Amagat)	$\int \alpha_{ca}(\nu) d\nu$ (cm ⁻¹ /cm)
12.2	32.7	0.218
"	65.5	0.407
"	99.1	0.607
"	129.0	0.782
"	164.8	0.967
"	207.2	1.139
"	268.2	1.417
32.7	22.1	0.388
"	37.8	0.658
"	49.9	0.887
"	63.6	1.122
"	77.4	1.408
"	90.4	1.592
"	115.0	2.011

These results are graphically represented in Fig. 9 where $(1/\rho_{O_2}) \int \alpha(\nu) d\nu$ was plotted against ρ_{O_2} for pure oxygen, and in Fig. 10 where $(1/\rho_{O_2} \rho_A) \int \alpha_{ca}(\nu) d\nu$ is plotted against ρ_A for the oxygen-argon mixture. In these plots straight lines were drawn using the method of least squares. From the plots it is observed that the integrated absorption coefficient can be represented by the equation,

$$(2) \quad \int \alpha(\nu) d\nu = \alpha_{0a} \rho_{O_2} + \alpha_{1a} \rho_{O_2}^2$$

for the case of pure oxygen where α_{0a} is the "intrinsic" absorption coefficient and α_{1a} is the binary absorption coefficient of pure oxygen and by the equation,

$$(3) \quad \int \alpha_{ca}(\nu) d\nu = \alpha_{1b} \rho_{O_2} \rho_A + \alpha_{2b} \rho_{O_2} \rho_A^2$$

for the oxygen-argon mixture where α_{1b} and α_{2b} are the binary and ternary absorption coefficients respectively of an oxygen-argon gas mixture.

It is noted that for pure oxygen the plot of $(1/\rho_{O_2}) \int \alpha(\nu) d\nu$ vs. ρ_{O_2} resulted in a straight line with positive slope and a small positive intercept on the $(1/\rho_{O_2}) \int \alpha(\nu) d\nu$ axis. The values of the coefficients in equation (2) were found to be:

$$\alpha_{0a} = (2.3 \pm 0.9) \times 10^{-3} \text{ cm}^{-2}$$

$$\alpha_{1a} = (5.93 \pm 0.17) \times 10^{-4} \text{ cm}^{-2}$$

where the limits of error are computed standard deviations. This non-zero value for α_{0a} may be interpreted as arising from allowed "intrinsic" transitions of the oxygen molecule due to its permanent magnetic dipole moment whose effect is small in comparison to the pressure induced effects. This magnetic dipole moment has been attributed to some of the electronic

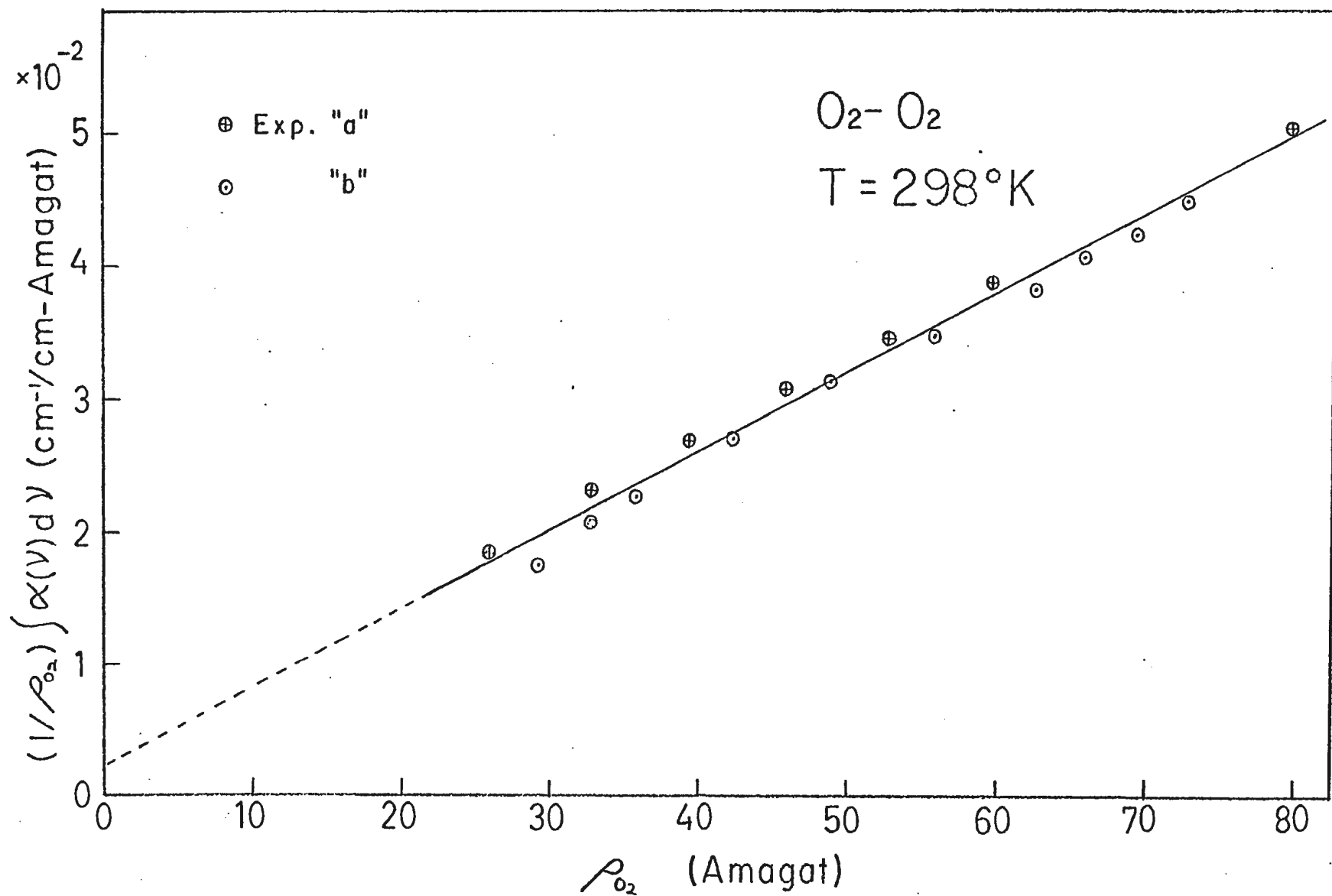


Fig. 9 The relation between the integrated absorption coefficient of the fundamental band of O_2 and the density of pure oxygen at $298^\circ K$.

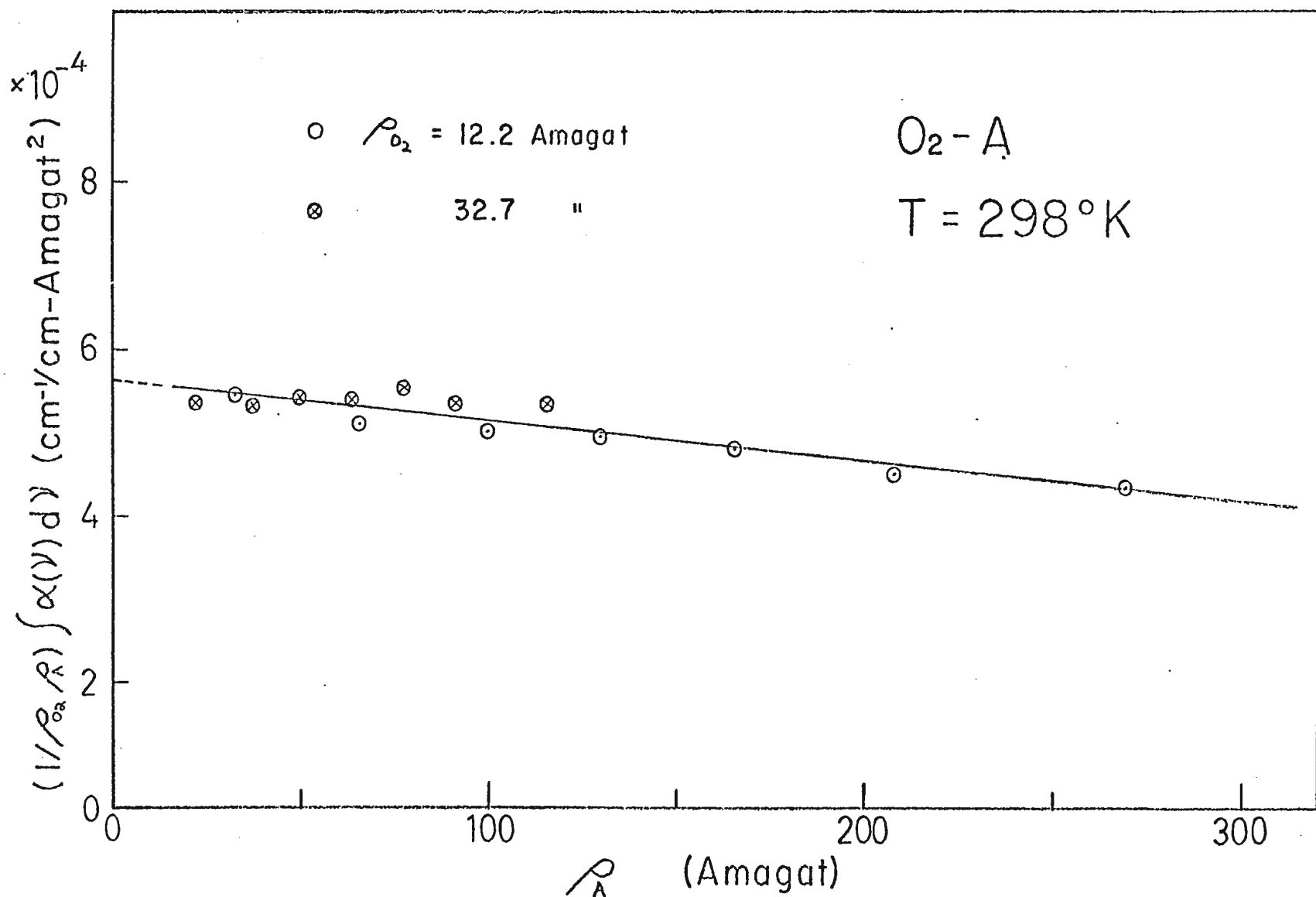


Fig. 10 The relation between the enhancement integrated absorption coefficient of the fundamental band of O_2 and the partial density of Argon in an $O_2 - A$ mixture at $298^\circ K$.

band systems of oxygen (e.g. Herzberg and Herzberg, 1947). It is however not possible to separate the portion of the band arising from the intrinsic transitions from the observed absorption contours in the present investigation since such intrinsic absorption is very weak in comparison with the pressure - induced absorption, and since it follows the same selection rules as the induced absorption. Existence of the fundamental band due to the magnetic dipole moment and the behavior of its absorption coefficients can only be studied with a very long absorbing path of oxygen at low pressures using a narrow spectral slit width. In the present investigation for the pure oxygen experiments, the lowest density of oxygen used was 25.9 Amagat at room temperature and 17.2 Amagat at low temperature. The existence of the intrinsic absorption coefficient may on the other hand be apparent only because of the presence of an undetected impurity in the oxygen gas used. A small intercept was also reported by Shapiro (1965) in his investigation of the fundamental band of oxygen in a lower density range of 2 to 12 Amagat with a path length of 40 to 80 meters. However, he attributed this result to the presence of an impurity such as water vapor. His value for α_{oa} determined from results obtained with a 40m path length is $(0.31 \pm 0.03) \times 10^{-3} \text{ cm}^{-2} \text{ Amagat}^{-1}$ compared with a value of $(2.3 \pm 0.9) \times 10^{-3} \text{ cm}^{-2} \text{ Amagat}^{-1}$ obtained in the present investigation. The difference in values is fairly large though not unreasonable since the contribution of this "intrinsic" absorption is very weak compared with the pressure induced

absorption. Consequently the accuracy in the measurement of the "intrinsic" absorption coefficient, α_{0a} is much less.

The observed coefficients α_{1b} and α_{2b} are presented in Table III together with α_{1a} . These were obtained by the method of least squares and the errors are the computed standard deviations. The binary absorption coefficients α_{1a} and α_{1b} arise due to binary collisions of oxygen molecules and those of oxygen and argon molecules respectively and the ternary absorption coefficient α_{2b} is due to the collision of one oxygen molecule and two argon molecules. For the pure oxygen, the ternary coefficient α_{2a} due to the collision of three oxygen molecules, was absent as expected since this coefficient would only appear at higher densities. The ternary term $\alpha_{2b} \rho_{O_2} \rho_A^2$ in equation (3) has been interpreted by previous authors (e.g. Hare and Welsh 1956) as being the combination of three effects: (a) the finite volume effect, (b) ternary collisions, and (c) the change of molecular polarizability with pressure. The effect of finite volume was discussed by Chisholm and Welsh (1954). At low densities the number of absorption inducing collisions is proportional to $\rho_{O_2} \rho_A$, however, when the volume of the molecules themselves becomes an appreciable fraction of the space which they occupy, the number of collisions increases more rapidly than the product $\rho_{O_2} \rho_A$. Secondly, when a molecule is surrounded by a symmetrical configuration of perturbing molecules the induced transition moment of the molecule is zero. Hence, ternary and higher order collisions

Table III

Observed absorption coefficients of the fundamental induced band of oxygen at 298°K and 201°K.

Temperature (°K)	Mixture	Binary Absorption Coefficient, $\alpha_{1a} + \alpha_{1b}$ ($10^{-4} \text{ cm}^{-2} \text{ Amagat}^{-2}$)	Ternary Absorption Coefficient, α_{2b} ($10^{-6} \text{ cm}^{-2} \text{ Amagat}^{-3}$)
298	O ₂ - O ₂	5.93 ± 0.17 (7.18 ± 0.04)	-
"	O ₂ - A	5.64 ± 0.08 (6.53 ± 0.12)	- 0.48 ± 0.06
201	O ₂ - O ₂	7.64 ± 0.22	-
"	O ₂ - N ₂	7.15 ± 0.26	2.0 ± 0.4
"	O ₂ - A	6.68 ± 0.30	0.2 ± 0.6

(Values in brackets are those obtained by Shapiro and Gush (1966))

would annul to some extent the action of binary collisions. This has been referred to as a "cancellation effect". Thirdly, a decrease in atomic and molecular polarizabilities at high densities was predicted by quantum mechanical considerations (Michels, de Boer, and Bijl 1937; de Groot and ten Seldam 1947). This would lower the integrated absorption coefficient to some extent but the magnitude of the effect is difficult to estimate.

It may be noted that another possible ternary term $\alpha_{2ab} P_{O_2}^2 / A$ due to collisions of two oxygen molecules and one argon molecule is missing in equation (3). This is probably due mainly to the limited experimental accuracy in the deduction of the present results and the smallness of the ternary coefficient α_{2ab} .

As seen in Table III the binary absorption coefficient for pure oxygen is greater than that for the oxygen-argon mixture and also the ternary absorption coefficient for the oxygen-argon mixture is negative which indicates the predominance of the "cancellation effect".

(2) The Low Temperature Experiments

The Absorption Profiles

Observed absorption profiles of the fundamental band of oxygen in pure gas at $T=201^{\circ}\text{K}$ are presented in Figure 11. The overall shape of the contours is similar to the room temperature contours in that they show pronounced Q and S branches and an indication of the O branch. The calculated positions of the band origin, ν_0 , and the O and S branch maxima agree well with the observed peak positions. As for the room temperature profiles, the positions of the computed individual rotational lines of the electric quadrupole spectrum are shown with the computed relative intensities indicated by the heights of the lines drawn. At this lower temperature of 201°K it is notable that the positions of the O and S branch maxima are closer to the band origin on the frequency axis than for the room temperature absorption and also the computed relative intensities of the O, Q and S branch maxima are slightly larger for the lower temperature. A normalization of a selection of low temperature absorption profiles for pure oxygen showed no change in their overall shape for the present range of densities. In Figure 12 two sets of normalized contours corresponding to the absorptions of pure oxygen at temperatures 201°K and 298°K are presented. Each profile represents an average absorption contour of three observed contours at a particular temperature which are normalized to give the same areas under the absorption

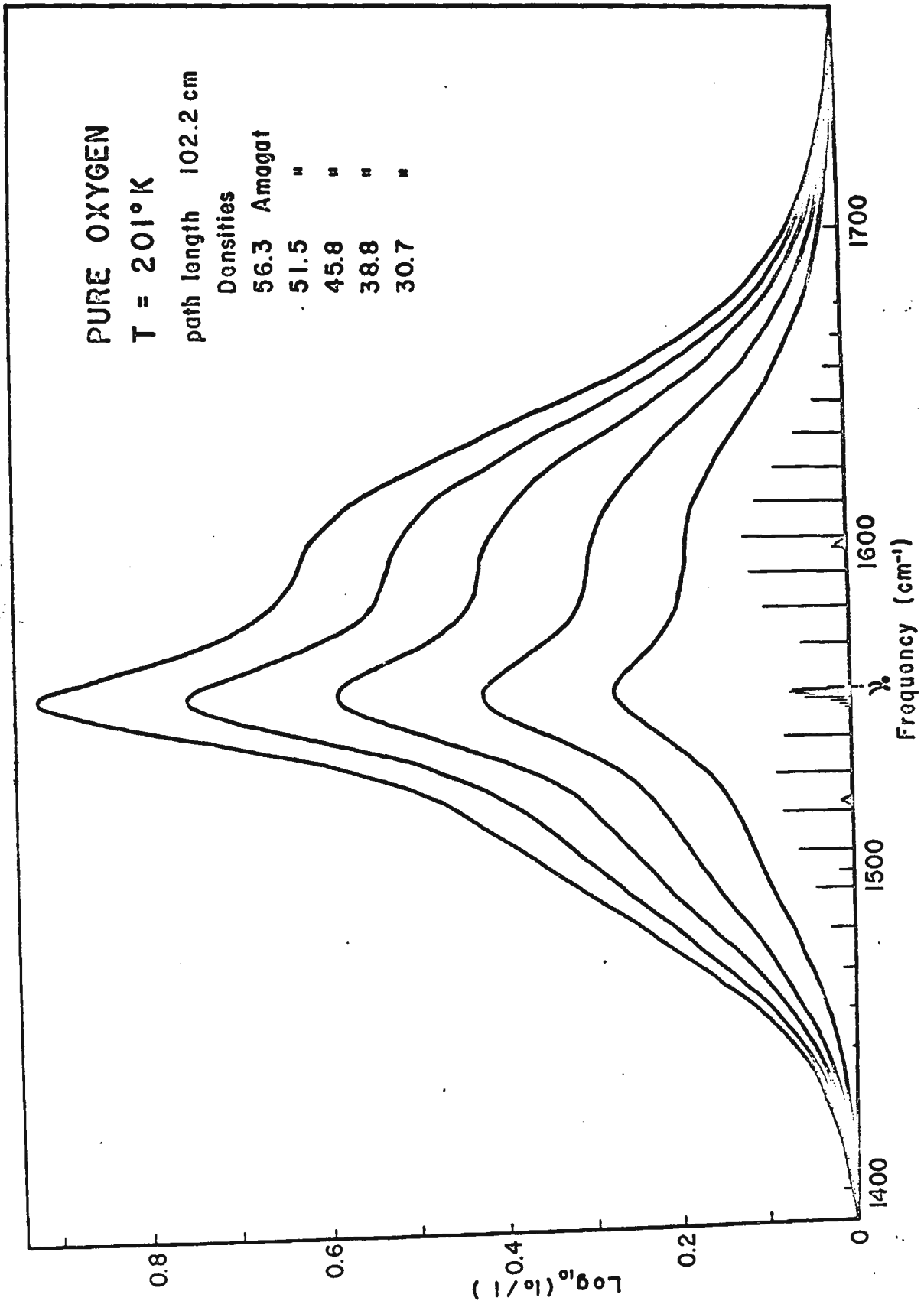


Fig. 11 The fundamental absorption band of oxygen at 201°K at various densities of gaseous oxygen.

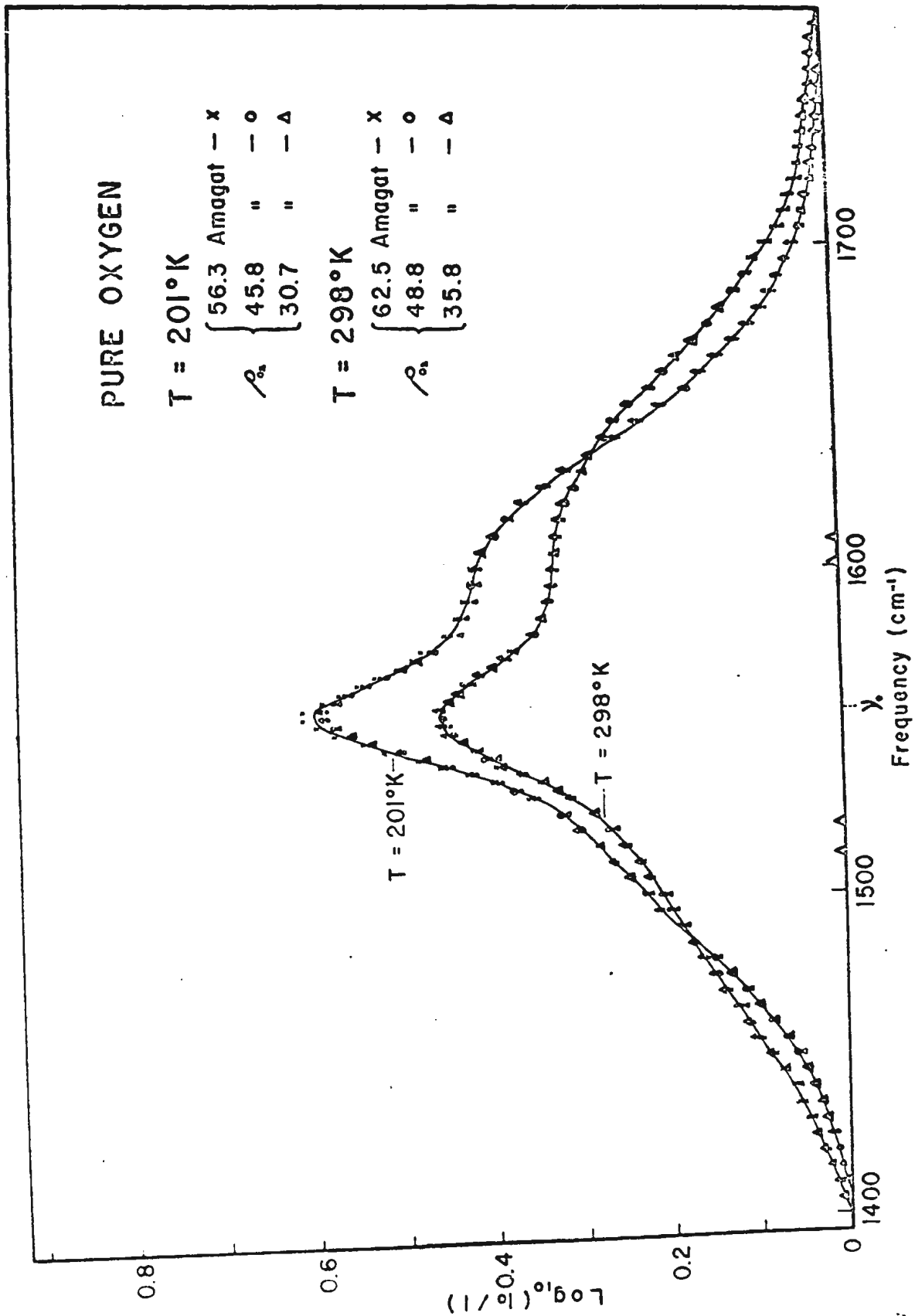


Fig. 12 The fundamental absorption band of oxygen at 298°K and 201°K in pure oxygen.

curves; two representative profiles at the corresponding temperatures with approximately the same areas under the absorption curves are compared. As seen in Figure 12, the overall absorption at 201°K is sharper than that at 298°K. The shift in the positions of the O and S branch maxima at the low temperature agrees well with the calculated values of the shifts, however, there was no observable shift in the position of the band origin, ν_0 at 1556 cm⁻¹, for the lower temperature.

Sets of observed enhancement absorption profiles in an oxygen-nitrogen mixture and an oxygen-argon mixture are presented in Figs. 13 and 14 respectively. The contours have a similar overall shape as those of the pure oxygen and show no observable shift in the positions of the O, Q, and S branch maxima. A normalization of a selection of contours for each of these two mixtures showed no change in the shape of the absorption band over the present range of densities.

A comparison of the absorption profiles of pure oxygen and the enhancement absorption profiles of oxygen-nitrogen and oxygen-argon mixtures at T = 201°K is shown in

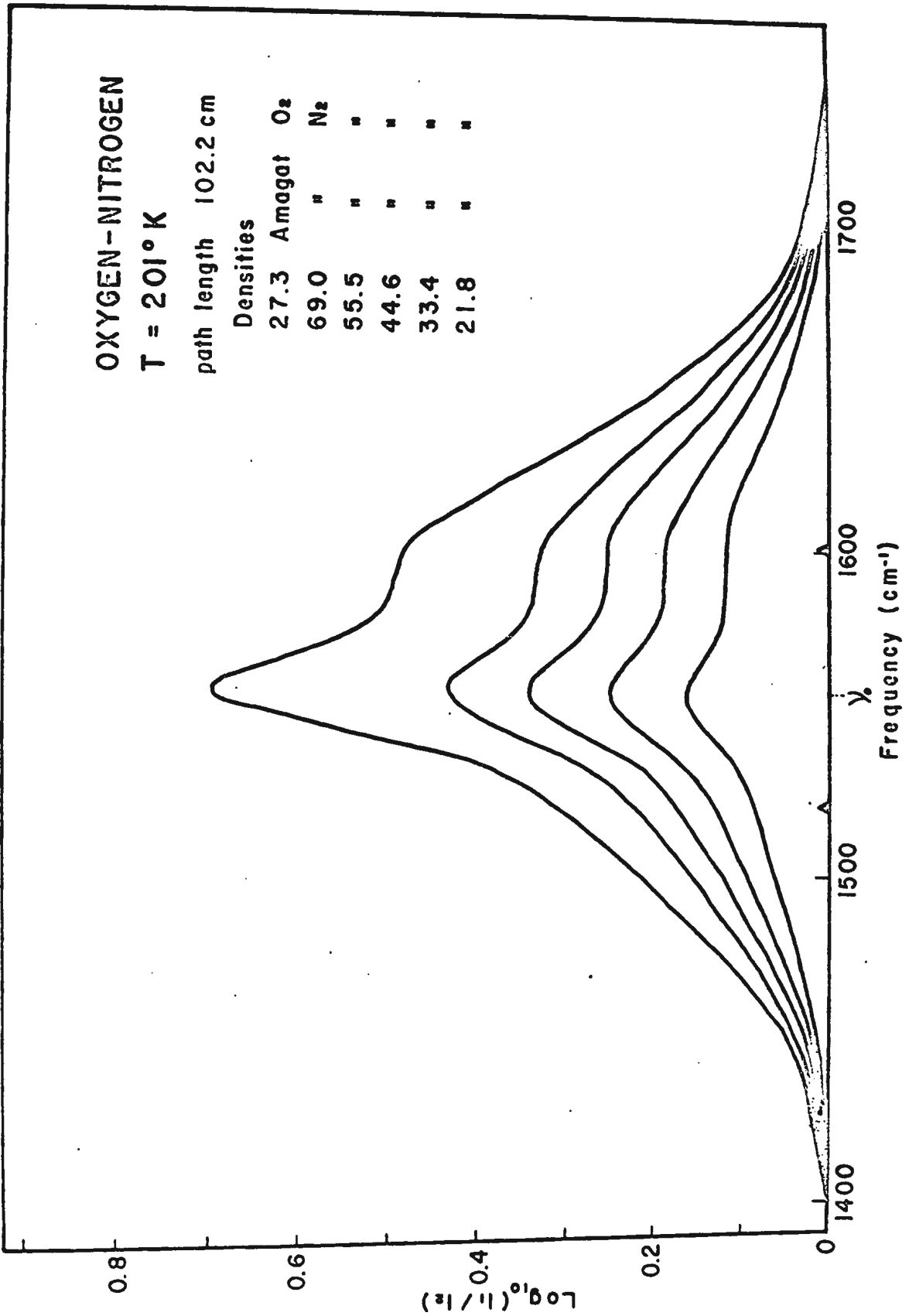


Fig. 13 Enhancement of the absorption of the fundamental band of oxygen at 201°K in an oxygen - nitrogen mixture.

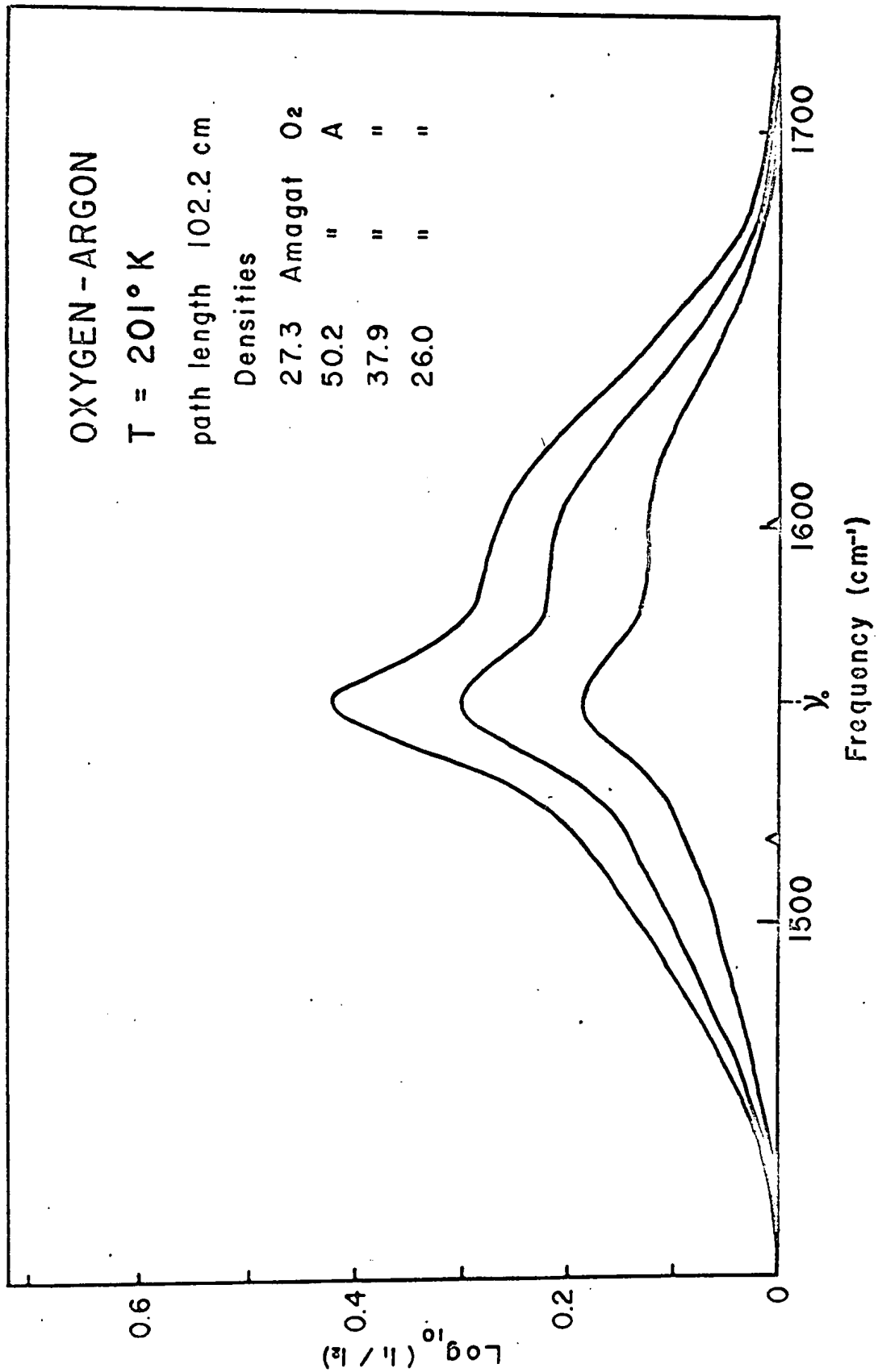


Fig. 14 Enhancement of the absorption of the fundamental band of oxygen at 201° K in an oxygen - argon mixture.

Figure 15. As before, these contours were chosen so that the products of the partial densities $\rho_{O_2}^2$, $\rho_{O_2}\rho_{N_2}$ and $\rho_{O_2}\rho_A$ were approximately the same for each contour. For the mixtures, the same base density of oxygen was also used. The pure oxygen and the oxygen-nitrogen contours are very similar in overall shape however they both differ from the oxygen-argon contour in that the Q branch is considerably sharper relative to the O and S branches for the oxygen-argon contour. It also shows that the total absorption in each contour is nearly the same for all three contours presented in Figure 15.

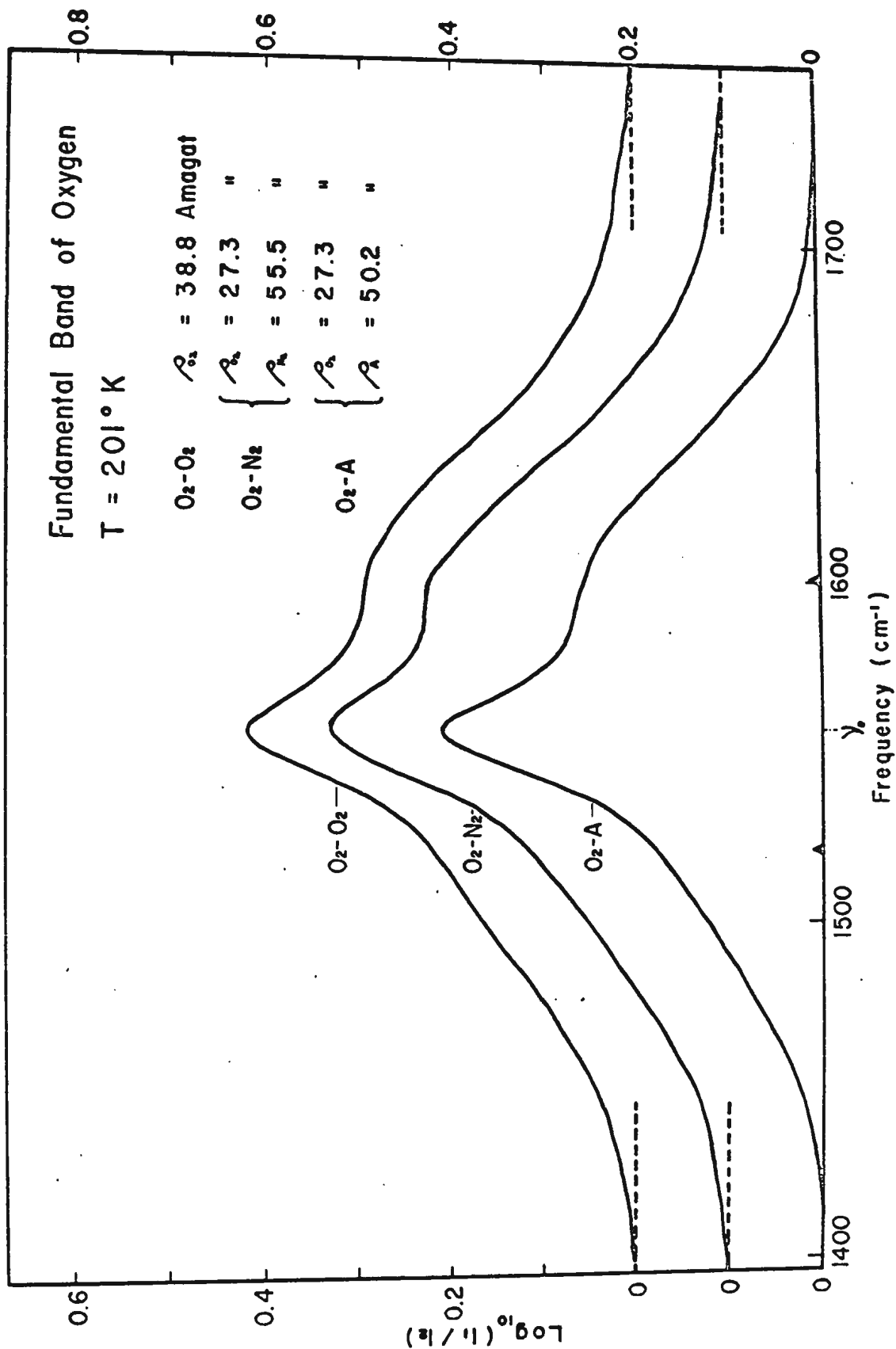


Fig. 15 The fundamental absorption band of oxygen at 201°K in pure oxygen, oxygen - nitrogen and oxygen - argon mixtures.

The Absorption Coefficients

The observed integrated absorption coefficients for pure oxygen, oxygen-nitrogen and oxygen-argon mixtures are summarized in Tables IV, V, and VI. These results are graphically represented in Figs. 16 and 17, where plots were made as in Part I of this chapter. For pure oxygen, a small positive intercept was obtained on the $(1/p_{O_2}) \int \alpha(\nu) d\nu$ axis as previously for the room temperature results. The equation for the straight line so obtained is

$$(4) \int \alpha(\nu) d\nu = (1.5 \pm 0.8) \times 10^{-3} p_{O_2} + (7.64 \pm 0.22) \times 10^{-4} p_{O_2}^2$$

The observed coefficients α_{1a} , α_{1b} and α_{2b} as described in Part I of this chapter are presented in Table III. It can be seen that the binary absorption coefficients decrease in the following order: pure oxygen, oxygen-nitrogen and oxygen-argon. For the oxygen-nitrogen mixture the ternary absorption coefficient is positive which is indicative of a predominant "finite volume effect". The ternary absorption coefficient for the oxygen-argon mixture is approximately zero at this low temperature but has a negative value at room temperature. This seems to indicate that at the low temperature the combined ternary effects have annuled each other while as stated previously at room temperature the "cancellation effect" is more predominant.

Table IV
Summary of Results
Pure O₂ , T = 201°K

ρ_{O_2} (Amagat)	$\int \alpha(\nu) d\nu$ (cm ⁻¹ /cm)
17.2	0.238
17.2	0.240
19.8	0.318
20.1	0.314
22.4	0.437
26.2	0.598
27.3	0.622
27.3	0.623
30.3	0.810
30.7	0.744
35.8	1.096
38.8	1.170
45.8	1.622
51.5	2.037
56.3	2.432
62.7	3.195

Table V
Summary of Results
 $O_2 - N_2$ Mixture , $T = 201^\circ K$

P_{O_2} (Amagat)	P_{N_2} (Amagat)	$\int \alpha_{en}(\nu) d\nu$ (cm^{-1}/cm)
17.2	32.1	0.455
"	47.8	0.687
"	67.2	0.966
"	84.0	1.268
"	102.1	1.586
27.3	21.8	0.450
"	33.4	0.693
"	44.6	0.938
"	55.5	1.204
"	69.0	1.729

Table VI
Summary of Results
O₂ - A Mixture , T = 201°K

P_{O_2} (Amagat)	P_A (Amagat)	$\int \alpha_{en}(\nu) d\nu$ (cm ⁻¹ /cm)
17.2	23.7	0.274
"	45.1	0.528
"	67.2	0.790
"	90.8	1.100
19.8	16.8	0.237
"	27.3	0.358
"	42.2	0.503
"	58.1	0.721
27.3	26.0	0.457
"	37.9	0.746
"	50.2	0.996

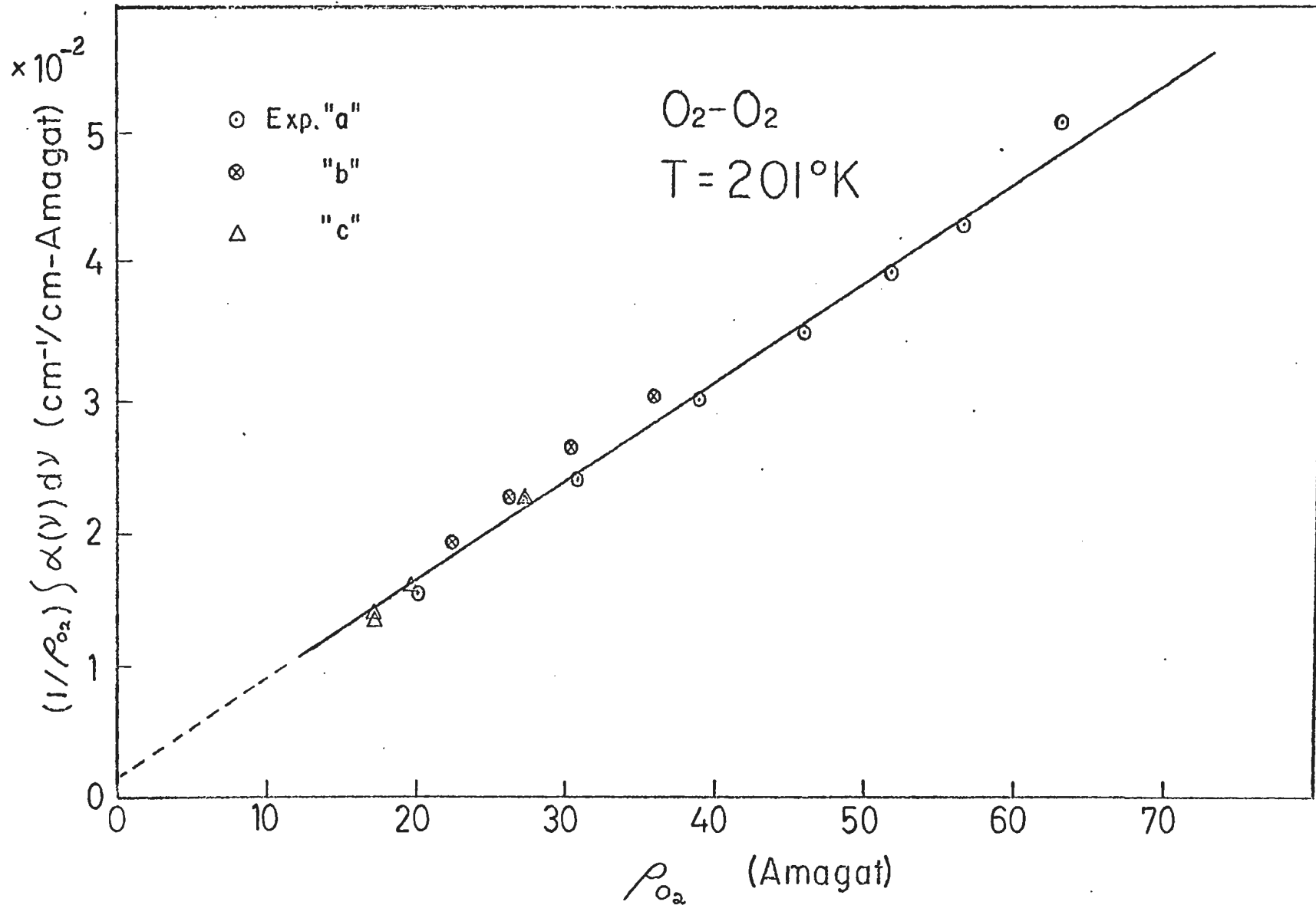


Fig. 16 The relation between the integrated absorption coefficient of the fundamental band of O₂ and the density of pure oxygen at 201°K.

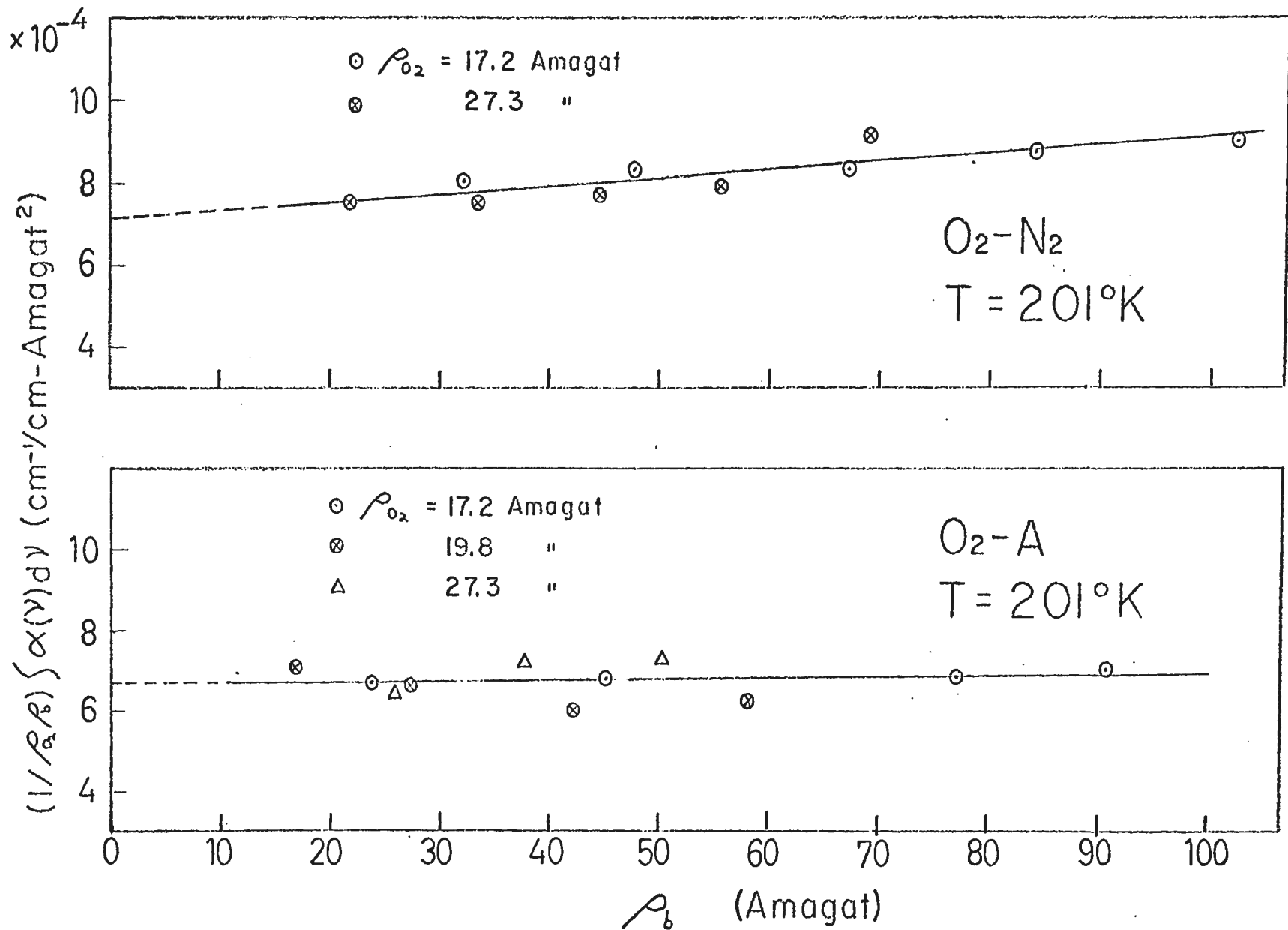


Fig. 17 The relation between the enhancement integrated absorption coefficients of the fundamental band of O₂ and the partial density of perturbing gas in O₂ - A and O₂ - N₂ mixtures at 201°K.

CHAPTER IV

THEORY AND DISCUSSION

Outline of Theory

The theory developed by Van Kranendonk (1957,1958) to explain the pressure induced infrared absorption of homonuclear diatomic molecules has since been used by many investigators and has proven to be most adequate. An outline of this theory is given in the present section and it is used to explain the experimental results obtained.

The experimental binary absorption coefficients α_{1a} or α_{1b} expressed in units of $\text{cm}^{-1}/\text{cm-Amagat}^2$ have to be converted to $\tilde{\alpha}_{1a}$ and $\tilde{\alpha}_{1b}$ respectively expressed in units of $\text{cm}^6 \text{sec}^{-1}$.

In this new form they are more directly connected to the transition probability arising from the dipole moments induced during binary collisions than to the observed integrated absorption intensity. The relationship between the above quantities may be shown in the following equations:

$$(5) \quad \tilde{\alpha}_{1a} = C \alpha_{1a} (V_0^2 / \bar{V} N_A^2)$$

$$(6) \quad \tilde{\alpha}_{1b} = C \alpha_{1b} (V_0^2 / \bar{V} N_A^2)$$

$$(7) \quad \text{where } \bar{V} = \int \alpha(\nu) d\nu / \int \nu^{-1} \alpha(\nu) d\nu$$

Here V_0 is the molecular volume at N.T.P., N_A is Avagadro number, C is the velocity of light and ν is expressed in cm^{-1} . \bar{V} for the oxygen fundamental band was found to be equal to 1571 cm^{-1} for the pure oxygen and oxygen-argon mixture at 296°K and equal to 1567 cm^{-1} for pure oxygen, oxygen-nitrogen, and oxygen-argon mixtures at 201°K . For pressure-induced absorption in oxygen-perturbing gas mixtures,

these new binary absorption coefficients can also be defined by the following equation,

$$(8) \quad c \int \alpha(\nu) \nu^{-1} d\nu = \tilde{\alpha}_{1a} \tilde{\rho}_a^2 + \tilde{\alpha}_{1b} \tilde{\rho}_a \tilde{\rho}_b + \tilde{\alpha}_{2a} \tilde{\rho}_a^3 + \tilde{\alpha}_{2b} \tilde{\rho}_a \tilde{\rho}_b^2 + \tilde{\alpha}_{2ab} \tilde{\rho}_a^2 \tilde{\rho}_b + \dots$$

where $\tilde{\rho}_a$ and $\tilde{\rho}_b$ are partial number densities (N/V) of absorbing gas a, and perturbing gas b; $\tilde{\alpha}_{1a}$ and $\tilde{\alpha}_{2a}$ are the binary and ternary absorption coefficients of the absorbing gas a; $\tilde{\alpha}_{1b}$ and $\tilde{\alpha}_{2b}$

are the binary and ternary absorption coefficients of a mixture of the absorbing gas a and perturbing gas b; $\tilde{\alpha}_{2ab}$ is the mixed ternary absorption coefficient. For the band in pure oxygen, equation (8) may be used by taking only the first term on the right hand side. Hence, equation (8) reduces to,

$$(9) \quad c \int \alpha(\nu) \nu^{-1} d\nu = \tilde{\alpha}_{1a} \tilde{\rho}_a^2$$

Here the term corresponding to the first order in $\tilde{\rho}_a$ does not appear in equation (8) because the equation represents the pressure-induced part of the absorption only.

For the mixture experiments where only enhancement absorptions were considered the equation becomes,

$$(10) \quad c \int \alpha_{en}(\nu) \nu^{-1} d\nu = \tilde{\alpha}_{1b} \tilde{\rho}_a \tilde{\rho}_b + \tilde{\alpha}_{2b} \tilde{\rho}_a \tilde{\rho}_b^2$$

In the present investigation the contribution of the binary absorption coefficient to the total absorption intensity of the band is predominant over the other contributions arising from the higher order terms since relatively low densities were used.

In the theory proposed by Van Kranendonk, the induced absorption in gases is treated similarly to the theory of the

equation of state of gases. The density expansion of the integrated absorption coefficients as in equation (8) is comparable to the virial expansion of the pressure where the second and third virial coefficients are the counterparts of the binary and ternary absorption coefficients. The integrated absorption coefficients provide information on the induced deformation of charge distribution of the molecules while the virial coefficients give information about the intermolecular forces.

For the determination of the density and temperature dependence of the binary absorption coefficients a suitable model for the induced dipole moment in a pair of molecules is assumed in terms of which the binary absorption coefficients are expressed. The model proposed by Van Kranendonk assumes a short range contribution which is angle-independent and decreases exponentially with R , and a long range contribution which is proportional to $1/R^4$ and depends on the orientations of the colliding molecules. R is the intermolecular separation. This model is known as the "exp-4" model; the induced absorption being attributed to the short range overlap induced dipole moment, due to the overlapping of electron clouds, and to the long range quadrupole induced dipole moment.

The binary absorption coefficient of a definite rotational branch B of the 0-1 vibrational band is given by Van Kranendonk (1957),

$$(11) \quad \tilde{\alpha}_{12}(B) = K \sum^{(B)} P_1 P_2 \int |\vec{M}(\vec{R}_{12})|^2 g_0(\vec{R}_{12}) d\vec{R}_{12}$$

Here K is defined by $K = \pi / 3m_0 \nu_0$, m_0 and ν_0 being the reduced mass and the frequency of the molecular oscillation respectively and P_1 and P_2 being the normalized Boltzmann factors for molecule 1 and molecule 2 respectively. \vec{R}_{12} is the intermolecular separation vector, $g_0(\vec{R}_{12})$ is the pair distribution function arising from (1,2) pair molecules, and $\vec{M}(\vec{R}_{12})$ is the induced moment of the pair of molecules (1,2).

In the "exp-4" model, the overlap moment is determined by two parameters ξ (or λ) and ρ giving the magnitude and range respectively. The long range moment is assumed to be dependant on the derivatives of the quadrupole moment and the average polarizability of the absorbing molecule at the equilibrium position, $Q'_1 = (\partial Q_1 / \partial r_1)_0$ and $\alpha'_1 = (\partial \alpha_1 / \partial r_1)_0$ respectively, and the quadrupole moment and the average polarizability of the perturbing molecule, Q_2 and α_2 respectively. Here r_1 is the internuclear distance. The components of $\vec{M}(\vec{R}_{12})$ are developed in terms of spherical harmonics and are found to be:

$$(12) \begin{cases} M_0 = \xi \exp(-K/\rho) + (3/2) \{ Q'_1 \alpha_2 (3 \cos \theta_1 - 1) - Q_2 \alpha'_1 (3 \cos \theta_2 - 1) \} R^{-4} \\ M_{+1} = (3/\sqrt{2}) (Q'_1 \alpha_2 e^{i\phi_1} \sin \theta_1 \cos \theta_1 - Q_2 \alpha'_1 e^{i\phi_2} \sin \theta_2 \cos \theta_2) R^{-4} \\ M_{-1} = (3/\sqrt{2}) (Q'_1 \alpha_2 e^{-i\phi_1} \sin \theta_1 \cos \theta_1 - Q_2 \alpha'_1 e^{-i\phi_2} \sin \theta_2 \cos \theta_2) R^{-4} \end{cases}$$

where θ_1, ϕ_1 and θ_2, ϕ_2 determine the polar angles of the internuclear axes of the molecules 1 and 2 relative to a coordinate frame xyz , the z -axis of which lies along the vector \vec{R}_{12} that connects the centre of mass of molecule 1 to

to that of molecule 2. From equations (11) and (12), the derived expressions for the binary absorption coefficients for the O, Q and S branches of the induced fundamental band in pure gas are:

$$(13) \quad \tilde{\alpha}_{1a}[O(J)] = (\mu_1^2 + \mu_2^2) \underline{J} \tilde{\delta} \cdot L_2 [O(J)]$$

$$(14) \quad \tilde{\alpha}_{1a}[Q(J)] = \lambda^2 \underline{J} \tilde{\delta} \cdot L_0[Q(J)] + \mu_1^2 \underline{J} \tilde{\delta} \cdot L_2[Q(J)] \\ + \mu_2^2 \underline{J} \tilde{\delta} \cdot L_0[Q(J)] \sum_{J'} \cdot L_2[Q(J')]$$

$$(15) \quad \tilde{\alpha}_{1a}[S(J)] = (\mu_1^2 + \mu_2^2) \underline{J} \tilde{\delta} \cdot L_2[S(J)]$$

where J is the rotational quantum number. For gas mixtures, these expressions are:

$$(16) \quad \tilde{\alpha}_{1b}[O(J)] = \mu_1^2 \underline{J} \tilde{\delta} \cdot L_2 [O(J)]$$

$$(17) \quad \tilde{\alpha}_{1b}[Q(J)] = (\lambda^2 \underline{J} + \mu_2^2 \underline{J}) \tilde{\delta} \cdot L_0 [Q(J)] \\ + \mu_1^2 \underline{J} \tilde{\delta} \cdot L_2[Q(J)]$$

$$(18) \quad \tilde{\alpha}_{1b}[S(J)] = \mu_1^2 \underline{J} \tilde{\delta} \cdot L_2 [S(J)]$$

In equations (13) to (18) the dimensionless parameters λ ,

μ_1 , μ_2 are defined as

$$(19) \quad \lambda = (\xi / e) \exp(-\sigma/\rho)$$

$$(20) \quad \mu_1 = Q_1' \alpha_2 / c \sigma^4, \quad \mu_2 = \alpha_1' Q_2 / c \sigma^4$$

where σ is the value of the intermolecular distance R for which the intermolecular potential is zero and e is the value of the electronic charge. $\tilde{\delta}$ is defined by

$$(21) \quad \tilde{\delta} = \pi e^2 \sigma^3 / 3 m_0 \nu_0$$

where m_0 and ν_0 are the reduced mass of the absorbing molecule and the frequency of the molecular vibration respectively.

The radial distribution integrals \underline{I} and \underline{J} are given by,

$$(22) \quad \underline{I} = 4 \pi \int_0^{\infty} \exp \{ -2(\chi - 1) \sigma / \rho \} q_0(\chi) \chi^2 d\chi$$

$$\underline{J} = 12 \pi \int_0^{\infty} \chi^{-6} q_0(\chi) \chi^2 d\chi$$

where $\chi = R/\sigma$ and $q_0(\chi)$ is the low density limit of the pair distribution function. Classically the pair distribution function is equal to $\exp(-V(x)/KT)$ and is quite valid at high temperatures. $V(x)$ is assumed to be the Lennard-Jones intermolecular potential energy function

$$(23) \quad V(x) = 4\epsilon (x^{-12} - x^{-6})$$

where ϵ is the depth of the potential. At intermediate temperatures quantum effects can be important and $q_0(x)$ may be expanded as an asymptotic series in powers of Planck's constant.

The resulting expressions for \underline{I} and \underline{J} are,

$$(24) \quad \underline{I} = \underline{I}^{cl.} - \Lambda^{*2} \underline{I}^{(2)} + \Lambda^{*4} \underline{I}^{(4)} + \dots$$

$$\underline{J} = \underline{J}^{cl.} - \Lambda^{*2} \underline{J}^{(2)} + \Lambda^{*4} \underline{J}^{(4)} + \dots$$

where $\Lambda^* = (h^2/2m\epsilon\sigma^2)^{\frac{1}{2}}$, m being the reduced mass of the pair of colliding molecules. $L_\lambda(B)$ in equations (13) to (18) is defined as,

$$(25) \quad L_\lambda(B) = \sum_{J, J'}^{(B)} P(J) L_\lambda(J, J')$$

where $\lambda = 0, 2$ and B corresponds to the various branches of the band. $P(J)$ is the Boltzmann factor for the rotational states normalized in such a way that,

$$(26) \quad \sum_{J=0}^{\infty} (2J+1) P(J) = 1$$

The quantities $L_\lambda(J, J')$ are Racah coefficients, the non-vanishing values of which for $\lambda = 0$ and 2 are given by:

$$(27) \begin{cases} L_0 (J, J) = 2J + 1 \\ L_2 (J, J - 2) = 3(J - 1) J / 2(2J - 1) \\ L_2 (J, J) = J(J+1)(2J+1) / (2J-1)(2J+3) \\ L_2 (J, J+2) = 3(J+1)(J+2) / 2(2J+3) \end{cases}$$

The total binary absorption coefficient of the band is obtained by adding equations (14), (15) and (16) for the pure gas and (17), (18) and (19) for the binary mixture after summation over J. In either case the result is the same,

$$(28) \quad \tilde{\alpha}_{1a} \text{ or } \tilde{\alpha}_{1b} = \lambda^2 \underline{I} \tilde{\gamma} + (\mu_1^2 + \mu_2^2) \underline{J} \tilde{\gamma}$$

Thus, according to the theory developed by Van Kranendonk the binary absorption coefficient can be expressed as the sum of two parts, one part is due to the short-range angle-independent electron overlap dipole moment and the other is due to the long range angle - dependant dipole moment resulting from the polarization of one molecule by the quadrupole field of the other. In equation (28), the term containing μ_1^2 is a result of the intensity due to single transitions, i.e. in the interaction process of two molecules, one molecule makes the transition $\Delta V = 1, \Delta J = 0, \pm 2$ while the energy of the other molecule remains unchanged, and the term containing μ_2^2 is due to the process involving double transitions in which one molecule of the interacting pair makes a vibrational transition only while the other molecule makes a rotational transition $\Delta J = 0, \pm 2$.

Calculation and Discussion of Results

With the aid of the equation (2b), the experimental values of $\tilde{\alpha}_{1a}$ and $\tilde{\alpha}_{1b}$ may be used to determine some of the molecular constants and parameters. Similar calculations have already been carried out by Keddy and Cho (1965) in the study of the fundamental band of nitrogen, and by Shapiro and Gush (1966) in the study of the fundamental bands of nitrogen and oxygen. In the present investigation, computational analysis of the observed binary coefficients was carried out to determine the derivative of the quadrupole moment of the oxygen molecule, Q' , and the overlap part of the absorption for each of the binary mixture systems under study.

As a preliminary step to such an analysis, the observed binary absorption coefficients $\tilde{\alpha}_{1a}$ at room temperature and at dry-ice temperature were first used. The observed values are $1.6 \times 10^{-35} \text{ cm}^6 \text{ sec}^{-1}$ for the room temperature experiments, and $2.0 \times 10^{-35} \text{ cm}^6 \text{ sec}^{-1}$ for the dry-ice temperature experiments. A simple inspection of the equation (2b) reveals that the right hand side of the equation as applied to the case of pure oxygen is temperature-dependent only through the distribution integrals \underline{I} and \underline{J} . Namely, the coefficients $(\tilde{\alpha}_{1a})_{298}^{\circ}$ and $(\tilde{\alpha}_{1a})_{201}^{\circ}$ obtained at room temperature and dry-ice temperature respectively, may be given by

$$(29) \quad (\tilde{\alpha}_{1a})_{298}^{\circ} = \lambda^2 \underline{I}_r \tilde{\gamma} + (\mu_1^2 + \mu_2^2) \underline{J}_r \tilde{\gamma}$$

$$(30) \quad (\tilde{\alpha}_{1a})_{201}^{\circ} = \lambda^2 \underline{I}_d \tilde{\gamma} + (\mu_1^2 + \mu_2^2) \underline{J}_d \tilde{\gamma}$$

where the suffices r and d are used to distinguish the distribution integrals for room temperature and dry-ice temperature respectively. Using the molecular constants and parameters given in Table VII, all the parameters contained in the right hand side of the equations (29) and (30) are determined except λ^2 , \underline{I}_r , \underline{I}_d and Q' of oxygen in the parameter μ_i^2 (cf. equation (20)). As shown in the equation (22), the value of the overlap distribution integral \underline{I} is dependent on the parameter ratio ρ/σ as well as on the reduced temperature T^* . It can also be shown from the equation (24) that $\underline{I} \approx \underline{I}_{cl}$ since Λ^* is small in the case of oxygen molecule (cf. Table VII) and thus the quantum correction can be considered negligible. In order to make a computational analysis of the results conforming with the theory of Van Kranendonk, it was therefore necessary to numerically compute \underline{I}_{cl} values at various T^* using different values of ρ/σ . The computed results obtained using IBM 1620 computer are plotted in Fig. 16. As a selected pair of values for \underline{I}_r and \underline{I}_d is substituted in the equations (30) and (31), the equations may be solved simultaneously to determine λ^2 and Q' . However, it was found that no pair of the values thus obtained represented any physical significance.

As another preliminary step, an attempt was also made to determine the parameters using the observed $(\tilde{\alpha}_{1a})_{298^\circ}$ and $\tilde{\alpha}_{1b}$ for O_2 -A mixtures at room temperature. This attempt also failed. It was therefore necessary to assume that the

Table VII

Molecular constants and parameters used in the calculations.

Temp. (°K)	Mixture	ϵ/k^a (°K)	σ^a (Å)	$\tilde{\gamma}$ ($\text{cm}^6 \text{sec}^{-1}$) $\times 10^{-32}$	$T^*/T/(\epsilon/k)$	Λ^*	\underline{J}^b	α_1/a_0^2	α/a_0^3	Q/ea_0^2
298	O ₂ - O ₂	117.5	3.58	1.77	2.54	0.199	12.1	5.0 ^c	11.0 ^c	0.30 ^d
"	O ₂ - A	118.7	3.49	1.64	2.51	0.200	12.1	-	11.1 ^c	0
201	O ₂ - O ₂	117.5	3.58	1.77	1.71	0.199	12.9	-	11.0 ^c	0.30 ^d
"	O ₂ - N ₂	105.7	3.64	1.87	1.90	0.213	12.6	-	11.8 ^c	1.1 ^e
"	O ₂ - A	118.7	3.49	1.64	1.70	0.200	12.9	-	11.1 ^c	0

a Hirschfelder, Curtis and Bird (1954)

b Van Kranendonk, J. and Kiss, Z.J., (1959)

c Stanbury, Crawford and Welsh (1953)

d Buckingham (1964) (Private communication)

e Reddy and Cho (1965)

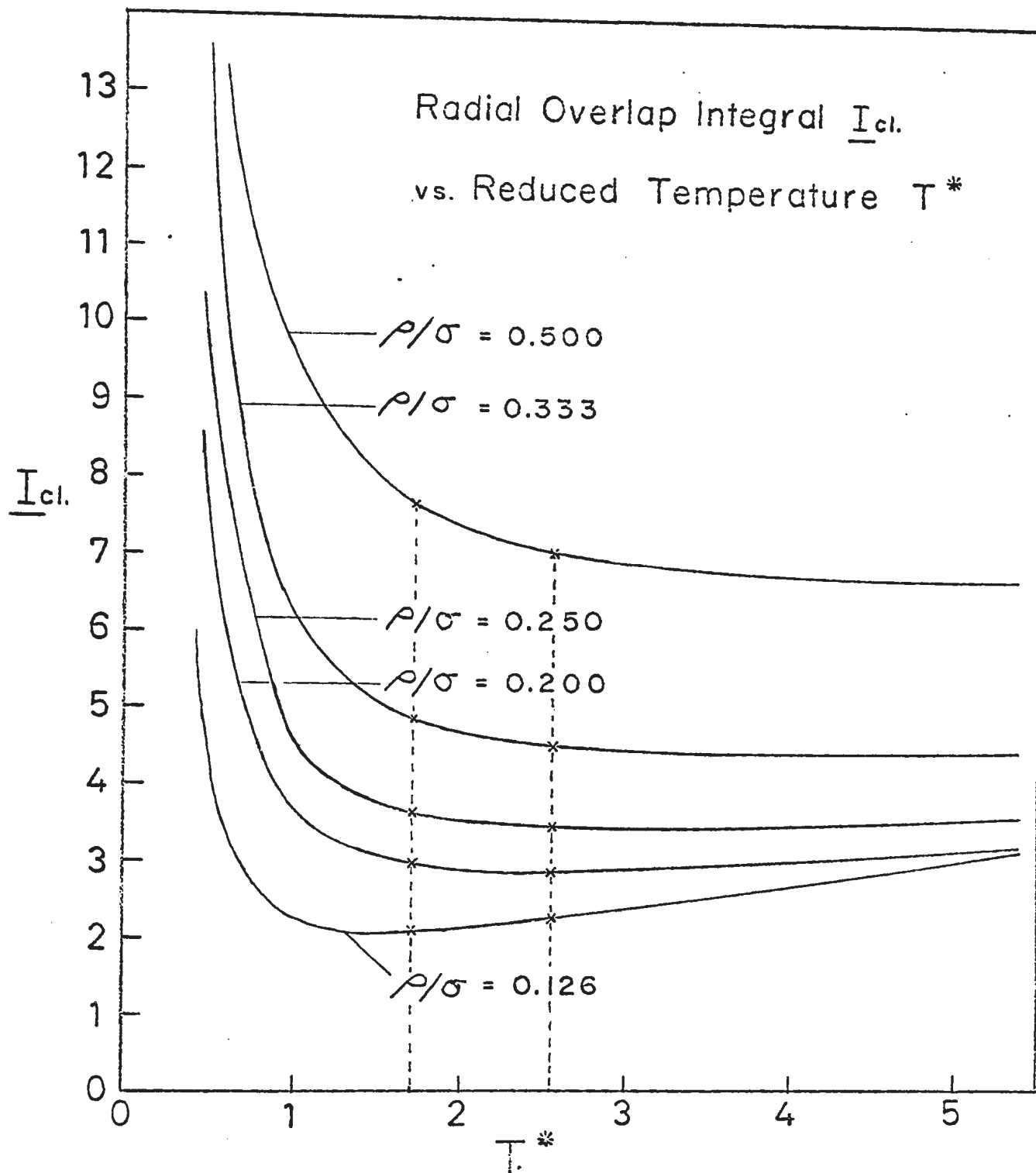


Fig. 18 Numerically computed classical part of the overlap configurational integral. (Broken lines indicate the reduced temperatures of 1.71 and 2.54 for pure oxygen at dry-ice and room temperatures respectively.)

absorption bands observed in the present investigation are due entirely to the dipole moment induced by the quadrupole interactions. This assumption is qualitatively justified further by the facts that (1) the computed absorption intensities arising from the quadrupole moment show in general good agreement with the observed bands in pure oxygen without any indication of an unaccounted large intensity in the Q branch, and (2) the enhancement absorption in the $O_2 - He$ mixture which can be considered to arise mainly from the overlap interaction, could not be observed at total pressures up to 3000 psi. at the low temperature. The polarizability of the helium molecule is very small and consequently the quadrupole contribution to the binary absorption coefficient should be small.

Upon the above assumption the equation (28) may be re-written by

$$(31) \quad \tilde{\alpha}_{1a} \text{ or } \tilde{\alpha}_{1b} = (\mu_1^2 + \mu_2^2) \underline{J} \tilde{\gamma}$$

Applying the equation (31) to all the experimentally determined binary coefficients, Q' of the oxygen molecule was determined for each case. The value of Q' thus obtained was $1.6 ea_0$ for all cases except for the $O_2 - A$ mixtures at room temperature and for the pure oxygen at the low temperature where values of $1.5 ea_0$ and $1.8 ea_0$ were obtained respectively. Here e is the electronic charge and a_0 is the first Bohr radius of the hydrogen atom. The value obtained in the present investigation agrees well with the value by Shapiro and Gush (1966) whose average value of Q' was found to be $1.6 ea_0$.

The binary absorption coefficients of the band in pure oxygen and in various mixtures were computed using the value of $Q' = 1.6 ea_0$, and are presented in Table VIII with the observed values for the purpose of comparison. As expected, the agreement between the computed and experimental values is good except for pure oxygen at 201°K . For the band in pure oxygen at 201°K , it can be seen that the difference between the computed and experimental values, $0.4 \times 10^{-35} \text{ cm}^6 \text{ sec}^{-1}$, represents one fifth of the observed coefficient.

This increase may lead to the following considerations:

(1) The increase in the absorption may be due to the overlap interaction of the type proposed by Van Kranendonk. The contribution to the absorption is considered to be additive. A simple calculation, using the value of the integral \underline{I} with $\rho/\sigma = 0.126$, reveals that the overlap parameter λ^2 has the value as high as 10.9×10^{-5} . It is highly improbable that the such strong overlap interaction should not be detected at room temperature. The theoretical value of the absorption arising from the overlap interaction, $\lambda^2 \underline{I} \tilde{\nu}$, does not alter much at the two temperatures since the temperature variation of \underline{I} is not more than 10% in the present range of temperature. It is also worth noting that the shape of the absorption contour at the low temperature does not show any indication of unproportionate increase in the Q branch, which may arise from the angle-independent overlap interaction.

Table VIII

Summary of Calculations

Temp. (°K)	Mixture	$\mu_1^2 \underline{J} \tilde{\gamma}^*$ (cm ⁶ sec ⁻¹) x 10 ⁻³⁵	$\mu_2^2 \underline{J} \tilde{\gamma}$ (cm ⁶ sec ⁻¹) x 10 ⁻³⁵	Total (cm ⁶ sec ⁻¹) x 10 ⁻³⁵	Observed $\tilde{\alpha}_{1a}$ or $\tilde{\alpha}_{1b}$ Total (cm ⁶ sec ⁻¹) x 10 ⁻³⁵
298	O ₂ - O ₂	1.5	1.1 x 10 ⁻²	1.5	1.6
"	O ₂ - A	1.7	0	1.7	1.5
201	O ₂ - O ₂	1.6	1.2 x 10 ⁻²	1.6	2.0
"	O ₂ - N ₂	1.7	1.4 x 10 ⁻¹	1.8	1.9
"	O ₂ - A	1.9	0	1.9	1.8

* Values are obtained using $Q' = 1.6ea.$

(2) In the study of the fundamental band of hydrogen at low temperatures, a similar increase in intensity has been observed (Watanabe and Welsh 1965). Their investigations were able to explain the increase in terms of the formation of the molecular complex $(H_2)_2$ at low temperatures. The anomalous increase of intensity in the present investigation at the relatively high temperature of $201^{\circ}K$ may be explained in the following manner:

Since at lower temperature the relative kinetic energy of a colliding pair of oxygen molecules is smaller, the duration of the collision will increase proportionally. During the relatively long time of the collision, a third molecule colliding with the pair may aid the formation of the $(O_2)_2$ complex. The occurrence of such a formation may be greatly enhanced by the spin-interactions between the unpaired electrons present in each oxygen molecule. The probability of the formation of $(O_2)_2$ complexes may thus be quite sensitive to temperature variations. The absorption contour arising from the transitions by one component molecule in the $(O_2)_2$ complex or from the double transitions by both molecules of the complex cannot easily be estimated. However, it seems quite reasonable to assume that the increase of absorption intensity of pure oxygen at the dry-ice temperature is indicative of the formation of the $(O_2)_2$ complexes. It is noted that no increase of the similar nature was observed for the gas mixtures at the same temperature.

The first overtone band of oxygen, whose band origin frequency is approximately twice that of the fundamental band, has been observed to contain a portion which is due to the double transitions of oxygen molecules (Gush 1956). The double transition bands can be considered to be closely related to the $(O_2)_2$ complexes. It is therefore suggested that a study of the first overtone band of oxygen under similar experimental conditions as in the present investigation may lead to a firmer conclusion with regard to the existence of the $(O_2)_2$ complexes in the pure gas at the dry-ice temperature.

REFERENCES

- (1) Amagat, E. H. 1893. Ann. Chim. Phys. 29, 68.
- (2) Buckingham 1964. Private Communication.
- (3) Chisholm, D.A. and Welsh, H.L. 1954. Can. J. Phys. 32, 291.
- (4) Cho, C.W., Allin, E.J. and Welsh, H.L. 1963. Can J. Phys. 41, 1991.
- (5) Cho, C.W. 1958. Ph.D. Thesis, University of Toronto, Toronto, Ontario.
- (6) Cho, C.W. 1955. M.Sc. Thesis, University of Toronto, Toronto, Ontario.
- (7) Crawford, M.F., Welsh, H.L., and Locke, J.L. 1949. Phys. Rev. 75, 1607.
- (8) de Groot, S.R. and ten Seldam, G.A. 1947. Physica 13, 47.
- (9) Ellis, J.W. and Kneser, H.O. 1933. Physik 66, 583.
- (10) Gush, H.P. 1956. Ph.D. Thesis, University of Toronto, Toronto, Ontario.
- (11) Hare, W.F.J. and Welsh, H.L. 1958. Can. J. Phys. 36, 88.
- (12) Herzberg, L. and Herzberg, G. 1947. Astrophys. J. 105, 353.
- (13) Herzberg, G. 1950. Spectra of Diatomic Molecules, I. (D. Van Nostrand Co., New York).
- (14) Hilsenrath J. et al 1955. Tables of Thermal Properties of Gases, Natl. Bur. Standards (U.S.) Circ. 564.
- (15) Hirschfelder, J.O., Curtis, F.C., and Bird, R.B. 1954. Molecular Theory of Gases and Liquids. (Wiley, New York)

- (16) Janssen, J. 1886. C. R. 102, 1352.
- (17) Lewis, C.N. 1924. J. Am. Chem. Soc. 46, 2027.
- (18) Michels, A., de Boer, J. and Bijl, A. 1937. Physica, 8, 347.
- (19) Michels, A., Scharp, H.W. and De Graaf, W. 1954. Physica 20, 1209.
- (20) Michels, A., Wijker, H. and Wijker, H. 1949. Physica 15, 627.
- (21) Pai, S.T., 1965. M.Sc. Thesis, Memorial University of Newfoundland, St. John's, Newfoundland.
- (22) Reddy, S.P. and Cho, C.W. 1965. Can. J. Phys. 43, 793.
- (23) Shapiro, M.M., and Gush, H.P. 1966. Can. J. Phys. 44, 949.
- (24) Shapiro, M.M. 1965. Ph.D. Thesis, University of Toronto Toronto, Ontario.
- (25) Stanbury, E. J., Crawford, M. F., and Welsh, H. L. 1953. Can. J. Phys. 31, 954.
- (26) Smith, A. L., Keller, W. E. and Johnston, H. L. 1950. Phys. Rev. 79, 728.
- (27) Snook, C. 1962. M.Sc. Thesis, Memorial University of Newfoundland, St. John's, Newfoundland.
- (28) Stevenson, C. M. 1965. M.Sc. Thesis, Memorial University of Newfoundland, St. John's, Newfoundland.
- (29) Thomson, H. W. 1961. I. U. P. A. C.
- (30) Van Kranendonk, J. 1957 Physica 23, 825.

- (31) Van Kranendonk, J. 1958 Physica 24, 347.
- (32) Van Kranendonk, J. and Kiss, Z.J. 1959. Can. J. Phys. 37, 1187.
- (33) Watanabe, A. and Welsh, H. L. 1964. Phys. Rev. Letters 13, 810.
- (34) Watanabe, A. and Welsh, H. L. 1965. Can. J. Phys. 43, 818.
- (35) Welsh, H. L., Crawford, M. F., McDonald, R. E. and Chisholm, D.A. 1951. Phys. Rev. 63, 1264.

ACKNOWLEDGEMENTS

The research described in this thesis was supervised by Professor C. W. Cho to whom the author is greatly indebted for his guidance during the course of the experimental work and in the preparation of this thesis.

The author expresses his gratitude to Professor S.P. Meddy for his helpful advice in the course of the research and to Professor S. W. Breckon for his encouragement during the research work.

Thanks are rendered to Mr. Lee Wan-Fung and Mr. W. E. Russell for their assistance in some of the research work and also to the staff of the Department of Technical Services, Memorial University of Newfoundland, for their skillful workmanship and advice.

Financial assistance in the form of a Graduate Fellowship, awarded during the academic years of 1965-1966 was gratefully received from Memorial University of Newfoundland

The use of the computer facilities of the Mathematics Department of Memorial University of Newfoundland for the calculations is gratefully acknowledged.



M. U. LIBRARY

